Reaction Wheel Control of an Air-Bearing Floating Robot

Jorge Antonio Chavarín Montoya

Master of Science in Space Engineering

from the

University of Surrey

School of Computer Science and Electronic Engineering

Faculty of Engineering and Physical Sciences

University of Surrey

Guildford, Surrey, GU2 7XH, UK

September 2024

Supervised by: Nicola Baresi

DECLARATION OF ORIGINALITY

I confirm that the project dissertation I am submitting is entirely my own work and that any material used from other sources has been clearly identified and properly acknowledged and referenced. In submitting this final version of my report to the JISC anti-plagiarism software resource, I confirm that my work does not contravene the university regulations on plagiarism as described in the Student Handbook. In so doing I also acknowledge that I may be held to account for any particular instances of uncited work detected by the JISC anti-plagiarism software, or as may be found by the project examiner or project organiser. I also understand that if an allegation of plagiarism is upheld via an Academic Misconduct Hearing, then I may forfeit any credit for this module, or a more severe penalty may be agreed.

Reaction Wheel Control Of An Air-Bearing Floating Robot

Jorge Antonio Chavarín Montoya

Author Signature   Date: 10/09/2024

Supervisor's name: Dr. Nicola Baresi

WORD COUNT

Number of Pages: 65
Number of Words: 13406

ABSTRACT

The main objective of this project is to design and implement an Attitude Control System (ACS) utilizing a single-degree-of-freedom Reaction Wheel for an air-bearing floating robot owned by the Surrey Space Centre. This system controls the robot's simulating near-frictionless conditions like to those in space. The ACS uses mathematical models, control laws, and software-in-the-loop (SIL) testing to guarantee that the system meets operational standards.

The reaction wheel system, powered by a brushless DC (BLDC) motor, generates the torque required to adjust the robot's attitude. The BLDC motor allows precise control over the wheel's speed, which directly influences the accurate control of the robot's orientation. The CAD design and material selection were important steps for the smooth integration of all components, helping the system function as a whole.

The control law achieved in this project lets the system perform attitude adjustments and orientation changes with accuracy. Initial tests of the reaction wheel showed positive results, giving a solid base for implementing a functional prototype of the ACS as the next step.

This research contributes to the growing knowledge of attitude control systems for small satellites, such as CubeSats. The results are a control system that can be tested in real-time simulations, and a CAD model of the robot useful for future components integrations. This work has potential use in academic and industrial settings, especially in satellite development.

TABLE OF CONTENTS

LIST OF FIGURES

1 INTRODUCTION

Attitude control systems (ACS) are important for spacecraft and robotic platforms that need to function in frictionless environments. These systems help a satellite or robot reach and maintain the desired orientation, which is crucial for mission success. In this project, an ACS was designed and implemented for a floating robot that uses a reaction wheel as its main actuator.

The system's goal is to control the robot's orientation with high precision in real-time. This is accomplished by combining hardware components such as sensors and actuators with control algorithms tested through software-in-the-loop simulations, being the latter the main objective of this project. The floating platform, built to simulate microgravity conditions, provides a way to test the ACS's performance in real conditions.

1.1 Background and Context

In recent years, reaction wheel systems have become one of the most used attitude control systems for small satellites due to their accuracy capacity and no fuel necessity. Meanwhile, the need to test these and other spacecraft subsystems on the ground caused scientists to develop different ways to simulate space environments. Air-bearing spacecraft simulators have been used to test attitude determination and control systems for more than 45 years [1]. These robots use air-bearing technologies to float over surfaces, therefore simulating minimal torque environments.

Reaction Wheels are used to precisely orientate a small spacecraft in a desired direction, so they are tested in air-bearing floating robots. By using the principle of conservation of angular momentum, reaction wheels provide the required torque to adjust the robot's orientation in response to external disturbances or desired manoeuvres. The system comprises one or more motor-driven wheels mounted on the satellite's body that accumulate rotational energy. Any change in the angular acceleration of the wheel causes an equal and opposite reaction, thereby enabling the robot to achieve a specific angular momentum.

Space applications avoid mechanical contact, such as bearings, gears, or motor brushes. Consequently, brushless DC motors (BLDC) are becoming more relevant, as they have longer lifespan, higher torque and efficiency, and low heat dissipation than traditional DC motors [2].

The objective of this project is to design, manufacture, and test a single-degree-of-freedom reaction wheel system for a floating robot. With the aid of existing literature and practical observations, this research seeks to explain the fundamental principles, design considerations, and implementation challenges associated with the integration of a reaction wheel control system into ait-bearing floating robots.

1.2 Scope and Objectives

1. CAD design of air-bearing device equipped with a Reaction Wheel assembly, the model shall include a power source, a raspberry pi, and IMU unit, and a camera module to estimate the attitude of the "spacecraft", the reaction wheel and motor shall be sized and included in the model to enable attitude control experiments.

2. Develop a PID controller in MATLAB Simulink for the 1-DOF attitude control of an air-bearing robot on granite table by means of a reaction wheel.

3. The robot shall re-orient itself based on commanded "desired" attitude configurations, in Simulink simulations.

To achieve the first objective, a detailed CAD model of the air-bearing floating robot equipped with a reaction wheel assembly was created using SolidWorks. The design included a power source (LiPo Battery), a Raspberry Pi, a Gyroscope, and a camera module for estimate the robot's attitude. The reaction wheel and motor were sized and integrated into the model according to the robots wight and inertia measurements.

For the second objective, a controller was developed in MATLAB and Simulink to handle the 1-DOF attitude control of the robot using the reaction wheel. Main controller gains were deduced mathematically, and subsequent real-time simulations were performed to adjust the controller.

Finally, simulations were run to check that the robot could reorient itself based on user-commanded "desired" attitude configurations. The Simulink tests showed that the robot adjusted its orientation smooth and correctly, according to the input commands. While physical tests have yet to be completed, the simulations suggest that the system meets the expectations for this task..

1.3 Achievements

The main accomplishment of this project is the successful development of an Attitude Control System (ACS), which includes both mechanical design of its components and the CAD design of the floating robot SolidWorks. The 3D model created ensures the compatibility among its components and gives a framework for integrating future projects, making it easier to adapt or extend the system as needed. This model supports future work by offering a solid base for additional modifications.

Additionally, the mathematical model for the robot and the Acs, was used to simulate the dynamics of both plants. This model makes possible to predict the system's behaviour, forming the basis for the control law proposed in this project. It also offers valuable insight for potential improvements or alternative control strategies that could be explored in future research.

The project also achieved successful software-in-the-Loop (SIL) testing using Simulink and MATLAB. This testing confirmed that the developed control law functions effectively and helped in

fine-tuning it by running real-time simulations of the system's performance. Overall, these achievements lay a strong foundation for future development in attitude control systems for small platforms.

1.4   Overview of Dissertation

This dissertation is structured into several chapters and subchapters that describe the complete process from background review and conceptualization to implementation and testing of the system.

The first chapter provides the background and objectives of the project. It introduces the concept of Attitude Control Systems and explains why reaction wheels are a preferred solution for small platforms like CubeSats.

Chapter 2 gives an overview of the theoretical concepts and research that form the basis of the Attitude Control System. It also introduces the concept of floating robots as testing mechanisms for spacecrafts systems. Additionally, it covers attitude dynamics, reaction wheel operation and control laws used later in the project. The chapter reviews relevant literature on the use of reaction wheels in small satellites, which influenced the design choices made for the project.

The third chapter explains the physical and mathematical modelling of the floating robot. It includes a description of the robot's structural components, with CAD designs created in SolidWorks. This chapter also explains the decisions regarding material selection and measurements. It compares conventional DC motors with Brushless DC (BLDC) motors and discusses the advantages and challenges of using BLDC motors in space applications.

Subsequently, Chapter 4 dives into the attitude dynamics of the robot and the control strategies used to adjust its orientation. It describes the coordinate frames necessary to describe the robot's and components movements. Also, it focuses on the interaction between the reaction wheel and the robot, detailing how the wheel generates the torque required to rotate the robot. The mathematical models presented in this chapter serve as the basis for understanding the control laws developed later in the chapter.

Chapter 5 covers the simulation work performed to test the ACS, using Simulink. The control algorithms and models developed in the previous chapter are tested and evaluated in this section. This chapter also details the refinement of control strategies done through real-time testing.

Finally chapter 6 gives some conclusions about the complete report, evaluates if the main objectives were accomplished and give options for future work regarding reaction wheels.

2   BACKGROUND THEORY AND LITERATURE REVIEW

2.1   Air-bearing Floating Robots

Air-bearing floating robots have been used since the middle of last century to simulate microgravity conditions and spacecraft dynamics on Earth, becoming essential for developing and testing real space applications under controlled environments, such as attitude control systems or spacecraft manoeuvres.

This type of robot possesses air-bearings that create a thin layer of pressurized air between the spherical or planar surface of the robot and the surface on which it hovers, as shown in Figure 2-1. The pressurized air is expelled through small holes on the base of the robot, forming an air layer that drastically reduces the friction between the robot and the surface [3]. As a result, the robot can move freely in any direction with lower resistance, simulating the space microgravity environment.

The air system allows the robots to simulate an almost frictionless environment. By adjusting the pressure and direction of the air expelled, the movements of the robots can be controlled with precision, which allows them to replicate real dynamics conditions that objects would experiment with in space, such as the absence of gravity and atmospheric drag.
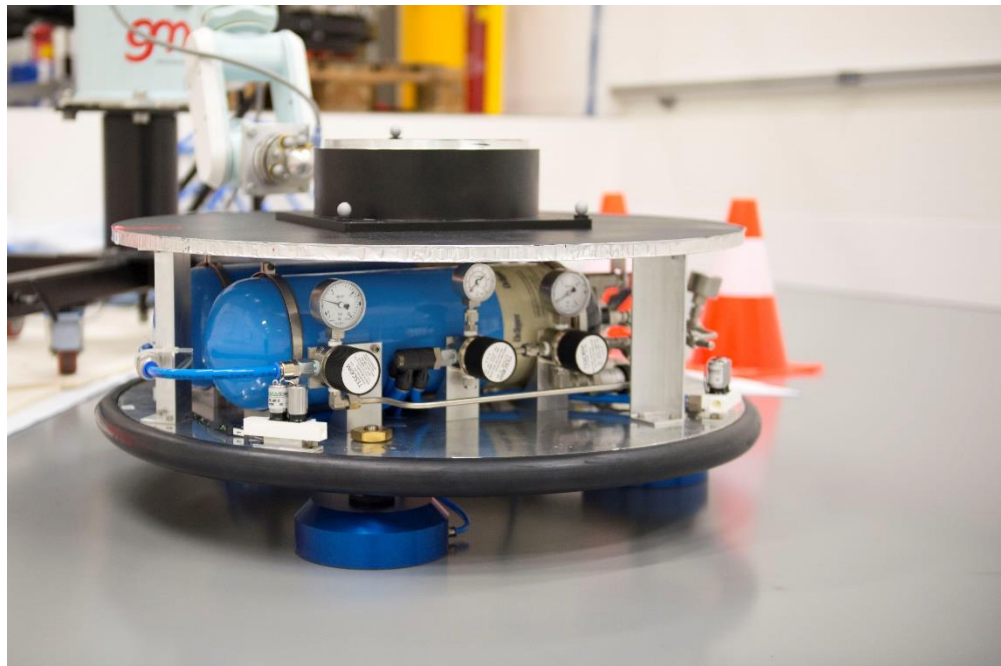
Figure 2-1 – ESA Air-Bearing Floating Robot. Credit: ESA-G/Porter – CC BY-SA 3.0 IGO [4].

Air-bearing platforms have evolved significantly over time. While early systems were initially designed for academic purposes, they quickly became indispensable for testing real spacecraft applications. Floating robots allows the simulation of rotational dynamics in an almost frictionless environment [1].

In recent years, the capabilities of air-bearing floating robots have improved thanks to technological advancements, enabling them to emulate more complex manoeuvres, such as multiple axes satellite rotations, without the friction restriction of Earth surfaces. Additionally, the continuous evolution of air-bearing floating robots reflects the growing interest in space exploration and their importance as space missions get more ambitious and challenging.

Floating robots have helped to develop new control law techniques, such as the ones used on reaction wheels, implemented mainly in CubeSats to maintain their stability and orientation. However, one of the main constraints is the scale of these spacecraft's simulators, typically limited to small or medium-size platforms, where emulating the dynamics of bigger spacecrafts still represents a challenge.

2.2   Attitude Dynamics

Attitude Dynamics refers to the study and control of orientation of a rigid body, relative to an inertial frame of reference or another object (such as the Earth or the Sun). This field is important for the stability and control of spacecrafts in space, as it determines how a spacecraft or satellite orientates its principal axes with respect to such reference frame. In order to realize specific tasks like antenna or camera pointing, or orbital manoeuvres, spacecrafts must be able to control their attitude.

The attitude of a satellite or spacecraft cand be defined through three main angles: roll, pitch and yaw, called Eule angles (ϕ, θ, ψ). Those angles describe the rotation of the spacecraft over its principal axes. Alternatively, rotation matrices or by an axis-angle vector (Euler axis and principal angle), that also describe the attitude of the spacecraft. Additionally, quaternions have some advantages in terms of describing rotations in a three-dimensional space avoiding singularities that Direction Cosine Matrices (DCM) have. The selection of the appropriate representation of the attitude is related to the requirements of the mission. While quaternions avoid mathematical singularities, Euler angles representation is the simplest method to describe a spacecraft attitude.

Furthermore, the equations of movement for attitude dynamics of a satellite can be described of how its orientation changes over time under the influence of external or internal torques. By controlling those torques the satellite could maintain or rotate to desired orientation. The equations of motion for the attitude dynamics derive from the Euler equations, that describe the rotational behaviour of a rigid body. Equation (2.1) relate the external torques acting in the spacecraft with the rate of change of its angular momentum:

$$\boldsymbol{\tau} = \dot{\boldsymbol{h}}_I = \dot{\boldsymbol{h}}_B - \boldsymbol{\omega} \times \boldsymbol{h} \tag{2.1}$$

Where:

- $\boldsymbol{h}$ is the angular momentum vector,

- $\boldsymbol{\tau}$ is the torque vector and,

- $\boldsymbol{\omega}$ is the angular velocity vector.

The subscript '**I**' on the equation above indicates a derivative in the *inertial* reference frame, and the subscript 'B' indicates derivative in the *body* frame.

Moreover, the angular momentum is a vector quantity that reflects the rotational motion of a body. Mathematically it can be defined as:

$$\boldsymbol{h} = \boldsymbol{I\dot{\omega}} \tag{2.2}$$

Where the inertia tensor of the body, $\boldsymbol{I}$, is matrix that represents how the mass of the satellite is distributed in relation to their axis of rotation. If the coordinate system of the body is aligned to its main axis, called principal axis of inertia, the matrix is diagonal, simplifying calculations associated with the rotation of the body:

$$\begin{bmatrix} I_{xx} & 0 & 0 \\ 0 & I_{yy} & 0 \\ 0 & 0 & I_{zz} \end{bmatrix} \tag{2.3}$$

Where I_{xx}, I_{yy}, and I_{zz} are the principal moments of inertia around the x, y, and z axes, respectively.

However, it the tensor of inertia is represented in a different coordinate system (i.e. when the mas of the body is not symmetrically distributed with respect to the principal axes), it is represented as:

$$\begin{bmatrix} I_{xx} & I_{xy} & I_{xz} \\ I_{yx} & I_{yy} & I_{yz} \\ I_{zx} & I_{zy} & I_{zz} \end{bmatrix} \tag{2.4}$$

The products of inertia, $I_{xy} = I_{yx}$, $I_{xz} = I_{zx}$, and $I_{yz} = I_{zy}$, indicate how the rotation around one of the axes is coupled with the rotation around another of axis.[5]

If we define the angular velocity vector as:

$$\boldsymbol{\omega} = [\omega_x \quad \omega_y \quad \omega_z]^T, \tag{2.5}$$

and assuming $\mathbf{X_B}$, $\mathbf{Y_B}$, $\mathbf{Z_B}$ are the principal axes of inertia, by substituting equation (2.2) in equation (2.1) and performing the cross product, the scalar quantity of the torque for each axis can be defined as:

$$\begin{aligned} \tau_x &= I_x \dot{\omega}_x + \omega_y \omega_z (I_z - I_y) \\ \tau_y &= I_y \dot{\omega}_y + \omega_x \omega_z (I_x - I_z) \\ \tau_z &= I_z \dot{\omega}_z + \omega_x \omega_y (I_y - I_x) \end{aligned} \tag{2.6}$$

In this project, the attitude control of the floating robot is done through a reaction wheel system, as the objective is to reorientate the robot into a desired direction.

2.3   Reaction Wheels

The principle of conservation of angular momentum establishes that in the absence of external torques, the angular momentum of a system remains constant. Reaction and momentum wheels take advantage of this principle to control and stabilize the orientation of the spacecraft. Both systems spin to generate a reaction torque that can change the orientation of the satellite without applying any external forces.

The main difference between them lies in their mode of operation. On one hand, reaction wheels are designed to adjust their rotational velocity to change the satellite's orientation. They are used to make precise manoeuvres by increasing or decreasing their angular velocity to generate an angular momentum that reorientates the spacecraft in the desired direction.

On the other hand, momentum wheels spin at a high and constant velocity, providing stability to the satellite. Their main function is to stabilize the attitude of the satellite against external disturbances, keeping it in a fixed orientation. While reaction wheels focus on the adjustment and active control of the attitude, momentum wheels centre on passive stabilization, resisting unwanted changes in orientation [6].

Reaction Wheels are a key component in spacecraft attitude control, as they can adjust and maintain spacecraft orientation very precisely [7]. Their simplicity and effectiveness have made them adopted in many space missions, from Earth observation satellites to deep space exploration.

The precise control of the spacecraft attitude by reaction wheels, without any external forces, allows the satellite to realize sustained operations in space, where other traditional methods involving thrusters would be limited by fuel consumption. Their capacity to generate a reaction torque internally improves the spacecraft's lifetime. Also, it contributes to the stability and manoeuvrability needed in complex operations, such as remote sensing operations and satellite alignment for communications.

Initial designs were big and limited in their operational range, which required high amount of power and were less flexible when performing manoeuvres. However, technology advances have led to the development of more compact, efficient, and durable systems. Modern reaction wheels operate at higher velocities, offering better control over the spacecraft's angular momentum and enabling more agile manoeuvres than before.

Integration of reaction wheel subsystems into spacecraft implies several considerations and engineering challenges. One of the principal problems is wheel saturation. This occurs when the reaction wheel reaches its maximum angular velocity and, therefore, cannot provide any extra torque. In order to mitigate this issue, reaction wheel subsystems are commonly complemented with magnetorquers or thrusters that work together with reaction wheels to desaturase them, restoring the capacity of the

wheel to provide torque. This combination ensures the continued capacity of attitude control [10].

Additionally, the configuration of the reaction wheels in the spacecraft depends on the specific requirements for each mission, where redundancy or failure tolerance must be considered. The three most common mount configurations of reaction wheels are *Three-Orthogonal Wheel Configuration*, *Four-Wheel Tetrahedral* (or *Pyramidal*) *Configuration*, and *Three-Wheel Skewed Configuration*. The first configuration is the simplest and widely used in missions where simplicity and power efficiency are paramount. In this configuration, the three wheels are aligned to the principal axis of the satellite (X_B, Y_B, Z_B), which allows them to control the attitude on the three axes with the minimum components possible. However, this design has no redundancy, meaning the control over one of the axes will be lost if a wheel fails.

Instead, the wheels are mounted at a non-orthogonal angle in the Four-Wheel Pyramidal Configuration, providing the satellite with complete redundancy. If one of the wheels fails, the remaining three wheels can still control the spacecraft's attitude. This configuration is the most used when reliability is of high importance.

Finally, the Three-Wheel Skewed Configuration, although it is more complex than the orthogonal configuration, offers an equilibrium between simplicity and limited redundancy. In this case, the wheels are mounted at specific angles, which allows a certain control level even with one-wheel failure without adding an extra wheel. This configuration is most suitable for missions with space and budget restrictions but requires some redundancy.

With the rise of small satellites, such as CubeSats, the need for smaller and lighter reaction wheels adjusted to space and power restrictions has emerged. Modern reaction micro-wheels maintain high performance despite their compact size, letting these new small satellites reach the same attitude control level as their bigger counterparts.

Furthermore, the design of satellites using *Commercial Off-the-Shelf* (COTS) components has gained popularity over the last few years, including reaction wheel systems. The use of COTS lets the owners reduce development costs and time by taking advantage of standard mechanics and electronic components that are easily available in the market. For the specific case of reaction wheels, BLDC and DC motors of high precision and electronic controllers are the most common and accessible options of COTS for reaction wheels. In this way, integration with external subsystems can be easily achieved using standards already used and tested in other industries. Even though the use of COTS implies certain limitations in durability or personalization of components, the technological advancements and high-quality components available in the market have made these options more viable for more space missions.

2.4   Linear Control Theory

Linear Control Theory is used to analyse dynamic systems described through linear differential equations. This theory is applied in control engineering to design systems that maintain stable behaviour and respond adequately to external perturbations. Representing these systems through equations in the state space gives a complete vision of their dynamics, considering inputs and outputs.

2.4.1   Controllability

A system is fully controllable if every state vector can be transferred from any initial state to any other state in a finite time through an adequate control signal. Mathematically, a continuous system described by:

$$\dot{x} = Ax + Bu \tag{2.7}$$

$$y(t) = Cx + Bu, \tag{2.8}$$

is fully controllable if the controllability matrix Q_C (see eq. 2.8) has a complete range. In other words, if the range is equal to the number of stated n, where the matrix A is a $n \times n$ square matrix.

$$Q_C = [B \quad AB \quad A^2B \quad ... \quad A^{n-1}B] \tag{2.9}$$

When the condition of full controllability is met, the system can be manipulated to reach any desired state [11].

2.4.2   Observability

The observability of a system refers to the capacity to deduct the complete state of the system from observing its outputs in a finite time. A system is fully observable if it is possible to determine the system's initial state with the information of the output $y(t)$ through time. Mathematically, a system described by equations (2.7) and (2.8) is fully observable if its observability matrix from equation (2.10) has a complete range.

$$Q_O = [C^T \quad A^T C^T \quad ... \quad (A^T)^{n-1} C^T]^T \tag{2.10}$$

Observability is especially important in systems where not all the states can be measured directly, and it is necessary to reconstruct the non-observable states from the available outputs.[11]

2.4.3   Full-state feedback controller

Through the full-state feedback controller, the system dynamics, like stability and response time, can be adjusted by using all the state variables, see Figure 2-2. This method is based on the relation:

$$u = -Kx, \tag{2.11}$$

where K is the gain matrix of the controller. With a correct designed of this matrix, it is possible to

locate the poles of the system in closed loop in desired locations of the complex plane, as long as the original system is fully controllable. This strategy is convenient when the dynamic behaviour of the system must be adapted to design specifications.[11].

To compute the matrix K, the eigenvalues of the closed-loop system must be replaced at desired positions to achieve the required performance. Given the state-space system from (2.7) and the control law (2.11), the closed-loop dynamics are expressed in (**2.12**), where r is the reference input [12]. The matrix K is selected toshift the eigenvalues of $A - BK$ to the desired locations.

$$\dot{x} = (A - BK)x + Br \tag{2.12}$$

This type of controller requires observability from all the states, which is not always feasible in practice. To address this, an observer is added to the system. This observer is responsible for estimating the non-measurable states from the system's outputs, thereby enhancing the controller's effectiveness.
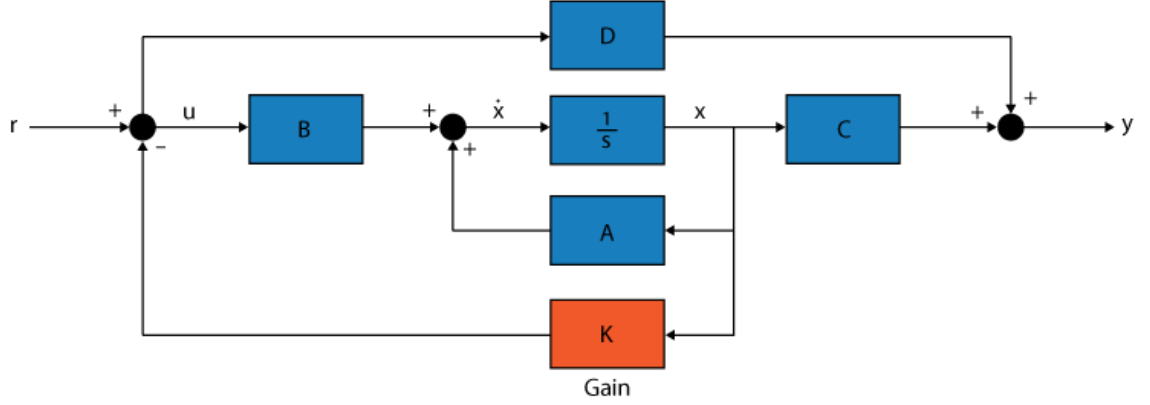
Figure 2-2 - Full-State Feedback Controller Block Diagram

2.5   MATLAB / Simulink

MATLAB is a high-level programming environment used for numerical computing, data analysis, and algorithm development. It provides various tools for tasks such as matrix operations, plotting functions and implementing algorithms, making it very useful for engineering and scientific applications. In this project, MATLAB was used to develop and simulate the state-space representation of both systems, to plot almost all graphs presented in this document, and to validate the controllability and observability of the system, among other functions that are annexed in APPENDIX B: MATLAB Scripts & Simulink Models.

Simulink is an extension of MATLAB that provides a graphical interface for modelling, simulating and analysing dynamic systems. In this project, Simulink was used to simulate the robot's attitude control system, including the reaction wheel, and the controller, in block diagram. Through Simulink, real-time simulations were performed to fine-tune the control algorithm and review the systems performance.

2.6   Summary

This chapter discussed the history and significance of air-bearing floating robots in simulating microgravity and space dynamics for satellite and spacecraft applications. Attitude dynamics was explored to describe how angular momentum can be used to rotate and change orientation of rigid bodies. Moreover, the functionality of reaction wheel systems, in terms of how they can control and stabilize satellites orientation by leveraging the principle of conservation of angular momentum and the benefits of the different mount configuration of reaction wheels were also boarded. Additionally, this chapter covered fundamental control concepts, such as controllability and observability and the Full-State Feedback Controller, that will be used in future chapters where the complete control of the system is going to be described.

3 ROBOT MODEL

3.1 Introduction

This chapter focuses on the design and implementation of the reaction wheel system as part of the air-bearing floating robot. A modular structure of various subsystems including a 2S-LiPo battery, a Raspberry Pi, and an inertial measurement unit (IMU), are integrated to the main structure of the floating robot from Surrey Space Centre. The reaction wheel, part of the Attitude Control system, was designed using SolidWorks, ensuring it meets the required moment of inertia for accurate control. This chapter delves into the CAD design, material selection and the integration of the reaction wheel with the motor, providing an overview of the processes involved in the design and manufacture of an Attitude Control system.

3.2 Air-Bearing Floating Robot

3.2.1 CAD Design

The robot was modelled using SolidWorks with the objective to get the necessary measurements for the design and integration of additional subsystems, such as the reaction wheel, and different sensors. The robot, property of Surrey Space Centre, had three air tanks, a pressure pump, three air-bearings, valves, and air hoses (see Figure 3-1). While most of the components' measurements were obtained directly from the manufacturer, some were unavailable, requiring physical measurements to be taken manually. The upper and lower disks were made of 1060 Aluminium Alloy, while the air tanks and valves were made of 316L Stainless-Steel to withstand high internal pressures.
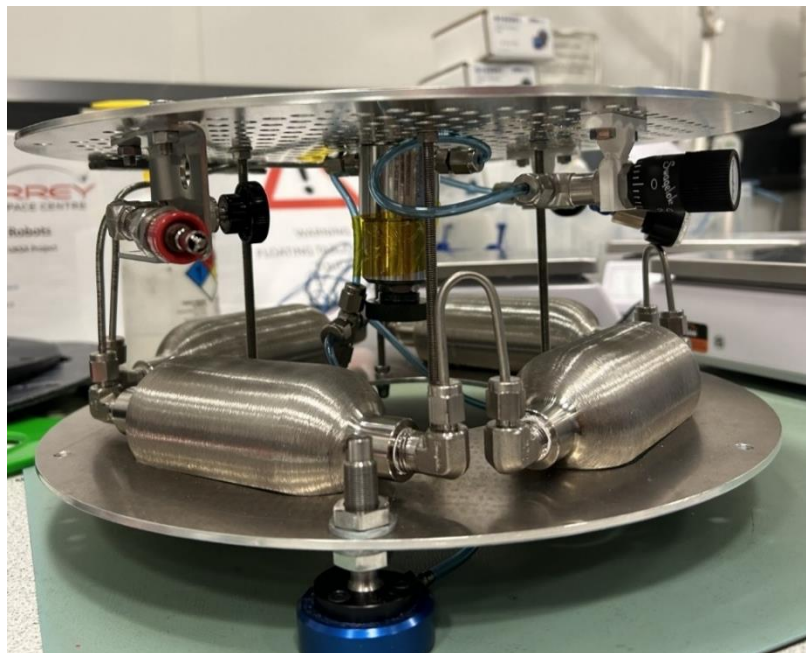
Figure 3-1 - Air-bearing Floating Robot from Surrey Space Centre

Once the main structure was modelled, electronics components were added, including a 2S-LiPo battery, a Raspberry Pi, a Pi-Cam, and the Inertial Measurement Module (IMU) along with their corresponding mounts. The structure of the robot was designed to be modular, with the power sub-system, sensors, On-Board Computer, and reaction wheel placed on different levels, following the CubeSat Standard (as shown in Figure 3-2).

The CAD model of the robot is fundamental for simulating of the entire system One of the challenges encountered was that the spacing between the holes on the top disk was not symmetrical and the valves were also mounted asymmetrically, causing misalignments in the centre of mass and the principal axes of inertia. A key strategy during assembly was to align the vertical axis of inertia and the centre of mass to the geometrical centre of the robot by carefully planning the distribution of components across the horizontal plane. The reaction wheel was positioned so that its axis of rotation was as closely aligned as possible with the principal axis of the robot.

Figure 3-2 - CAD Design with subsystems in distinct levels.

Finally, to align the centre of mass and the vertical principal axis of inertia to the vertical axis of the geometrical body, a pair of counterweights were added. Each counterweight was made of 316L-SS with a mass of 100.02 g and was placed in specific locations along the horizontal plane of the robot. Figure 3-3 shows the counterweights location on the top disk. The formula to calculate the position to place the counterweights in each axis is:

$$r_x = \frac{m_{robot} \cdot (-\Delta x)}{m_{cw}}$$

(3-1)

Where:

- r_x is the location of the counterweight in one axis,

- m_{robot} is the total mass of the robot,
- Δx is the misalignment of the centre of mass in the specific axis,
- m_{cw} is the mass of the counterweight.

The precision and correct alignment of the centre of mass are of importance to determine the proper behaviour of the robot particularly in the relation to the performance of the reaction wheel.
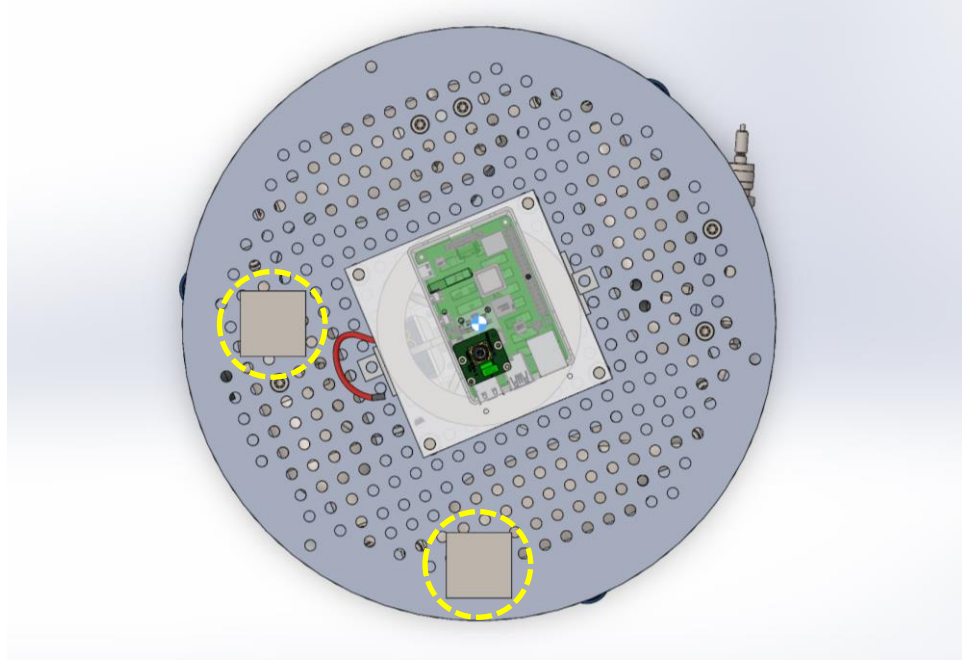
Figure 3-3 - Top-view of Robot showing counterweights circled in yellow.

3.2.2 Inertia measurements

From SolidWorks it was possible to obtain metrics of the robot, including weight, the Moments of Inertia, and the position of the principal axes of inertia with respect a reference frame (explained in the next chapter). SolidWorks name as X-axis to the minimum axis of inertia, and due to the distribution of weights, that is the vertical axis. Due to the inertial vertical axis was denominated as the Z-axis a rotation must be made. However, as the objective of the project is to rotate the robot only in its vertical axis, so just the scalar quantity of the Moment of Inertia in its X-axis is used.

Weight: 6.1299 kg,

Moments of Inertia:

$$I_x = 0.0511 \; {}^{kg}/_{m^2}$$

$$I_y = 0.0809 \; {}^{kg}/_{m^2} \qquad\qquad (3\text{-}2)$$

$$I_z = 0.0839 \; {}^{kg}/_{m^2}$$

3.3   Reaction Wheel Design

3.3.1   BLDC Motors vs DC Motors

DC Motors have been used for over a century, powering from small devices to industrial machines. However, as the demand for greater efficiency and control has grown, engineers have opted to use brushless DC motors (BLDC). These motors have outperformed standard DC motors in many applications, particularly in space, where precision and reliability are of great interest.

Traditional DC motors operate by interacting with a static magnetic field generated by a permanent magnet and a variable magnetic field produced by a coil in the rotor (see Figure 3-4). The rotor spins when its polarity changes, which is produced by a mechanical commutator with brushes that maintain contact with the rotating commutator [15]. This simple design allows easy speed and torque control by adjusting the voltage supplied to the motor.

Nevertheless, the mechanical commutator represents a potential point of failure because the brushes are subject to wear if there is no periodic maintenance, a problem in space applications where maintenance is not feasible.
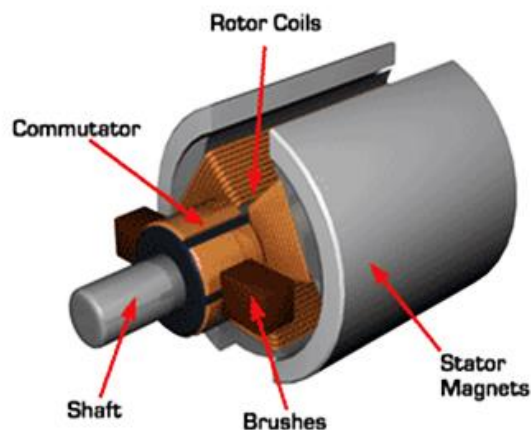
Figure 3-4 - Traditional DC brushed motor with a permanent magnet stator. Credit: ZGC Motor [13].

In contrast, BLDC Motors function with electronic commutation instead of mechanical. The rotor has a set of permanent magnets, and the coils are fixed on the stator. The commutation of current through the coils is managed electronically, which provides better control compared to DC motors and removes the risk of mechanical wear (see Figure 3-5) [15] [16].

Thanks to their robustness and precision, BLDC motors are well-suited for space applications. However, they require more complex control systems that includes sensors to detect the rotor position and electronic controllers to manage commutation and convert the input voltage into a three-phase voltage.
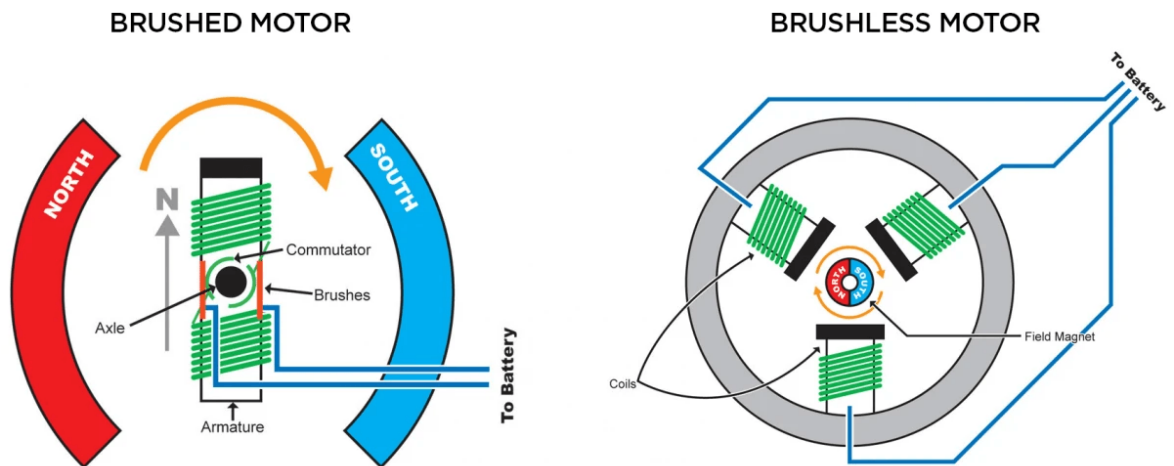
Figure 3-5 - Brushed Motor vs Brushless DC (BLDC) Motor [14].

Overall, BLDC motors offer a better efficiency -reaching up to 90%- due to the absence of energy loss brush friction. They are also lighter and more compact than their DC counterparts for the same power output. Brushless motors allow a more advanced control like velocity modulation or change of spin direction without additional components but are not as straightforward to control as DC motors.

The motor used for this project is a GM3506 Brushless. A BLDC was selected as they are more and more commonly used in space. GM3506 is powerful and reasonably priced, ensuring it can produce the necessary torque to spin the wheel. Additionally, the motor has incorporated an AS5048A Encoder, with two types of communication, PWM or I2C, which was another reason to select it. Table 3-1 shows the specifications of the motor.

Figure 3-6 - GM3506 BLDC Motor with AS5048A Encoder integrated [17].

Spec.		Value
Resistance		5.6 Ω ± 5%
Weight		80.3 g
No Load	Voltage	16 V
	Current	0.17 ± 0.05 A
	Max. Speed	2149 – 2375 RPM
Load	Voltage	12 V
	Current	1 A
	Torque	600 – 1000 g*cm

Table 3-1 - Motor GM-3506 Specifications.

The 2S-LiPo battery provides power to the motor, ensuring the motor can provide its maximum torque indicated in the datasheet.

The maximum torque of the motor, according to Table 3-1, is $\tau = 600\ g * cm = 0.059\ Nm$. The acceleration of the robot is calculated from the below equation:

$$\alpha = \frac{\tau}{I_{robot}}$$
(3-3)

Substituting the inertia of the robot in the vertical axis (I_x), calculated at eq.(3-2), the maximum angular acceleration that the robot can have is $\alpha = 1.154\ rad/_{s^2}$.

Lastly, using equation (**3-4**) the minimum time taken by the robot to execute a complete rotation ($\theta = 2\pi$) is $t = 3.3\ seconds$, this can be very fast, however a condition in the control loop can be added to limit the torque produced by the motor.

$$t = \sqrt{\frac{2\theta}{\alpha}}$$
(3-4)

3.3.2 Wheel measurement & material selection

The wheel design includes a spoke structure in a 45-degree distribution to reduce its overall weight while concentrating most of the mass in the outer ring compared to the disk-ring structure. The minimization of mass in the centre of the wheel, thanks to the spokes design, contributes to a more efficient operation of the motor due to the reduction of the load on it. The radius of the outer and inner circles of the ring are $r_{out} = 55\ mm$ and $r_{in} = 40\ mm$, respectively, and a depth of $h = 30\ mm$. The inner disk radius is $r_{disk} = 45\ mm$, see Figure 2-1. Eight spokes join ring and disk.
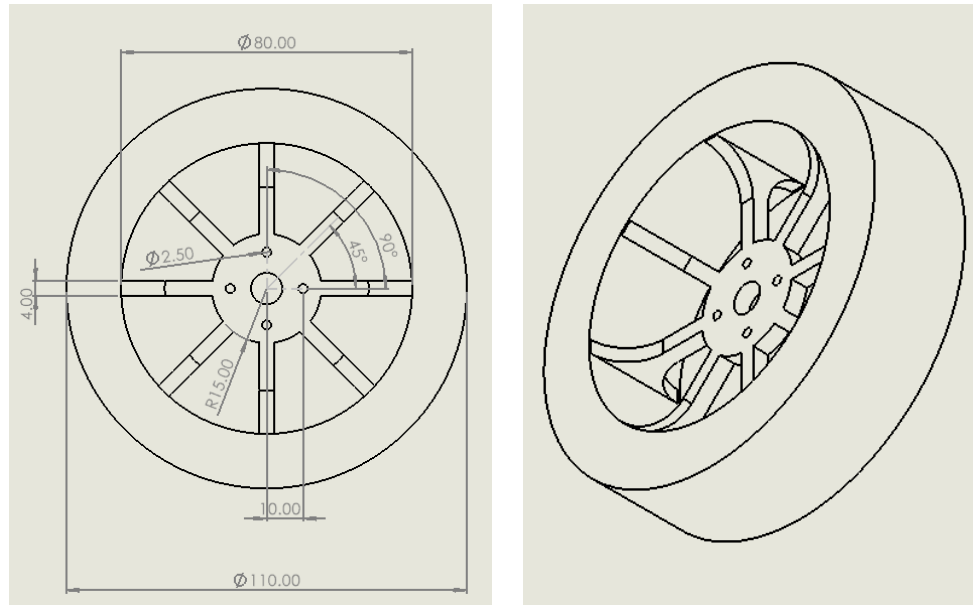
Figure 3-7 – 2-D Drawing of Reaction Wheel. Measurements in mm.

The reaction wheel was manufactured of 316L stainless steel because of its excellent resistance to corrosion. Additionally, its high density allows smaller designs with high inertia. However, it is also a good practice to use an aluminium alloy, depending on the mission.

The wheel design requires to take in consideration the physical and dynamic properties of the system.

3.3.3   CAD Design

The wheel design was also carried out using SolidWorks, with the objectives of calculating the wheel's moment of inertia, manufacturing the wheel, and finally assembling it to the robot. The wheel, as shown in Figure 3-8, has a central hole in the inner disk to couple it into the motor through a shaft, and four smaller holes around (diameter = 1.25 mm) for screws to securely attach the wheel to the motor, preventing any non-desired movement.
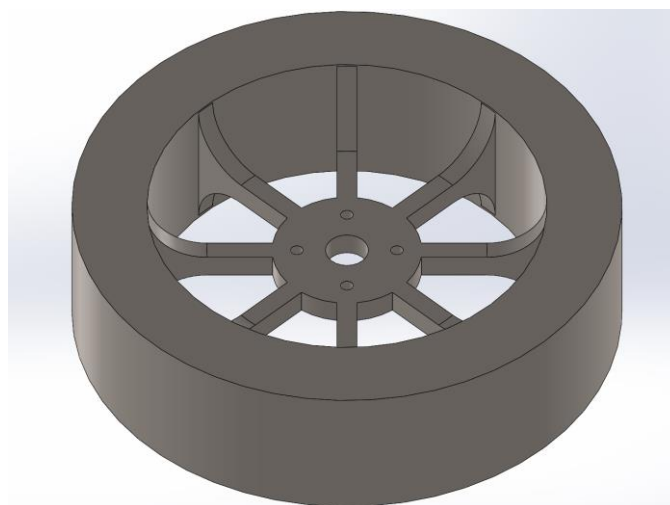
Figure 3-8 - Wheel CAD

The width of the spokes and the outer ring of the wheel were adjusted to achieve the desired moment of inertia. Figure 3-8 shows the wheel, while Figure 3-9 displays the complete reaction wheel assembly.
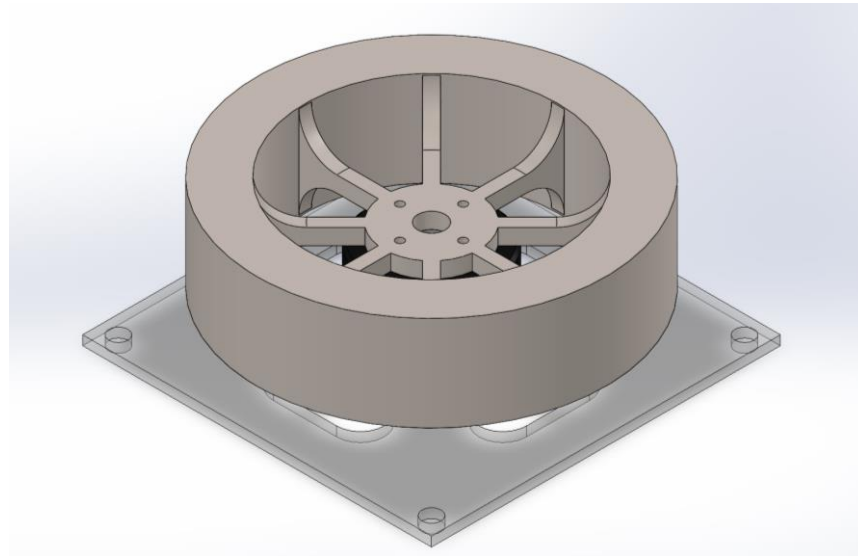
Figure 3-9 - Reaction Wheel System Assembly

The base of the motor (Figure 3-10) positions the reaction wheel system at the centre of the robot, aligning both vertical axes. The base includes four elliptical holes, with a semi-major axis of 17.5 mm and a semi-minor axis of 7.5 mm, to pass the wires from the battery to the motor and to the raspberry in the upper level.
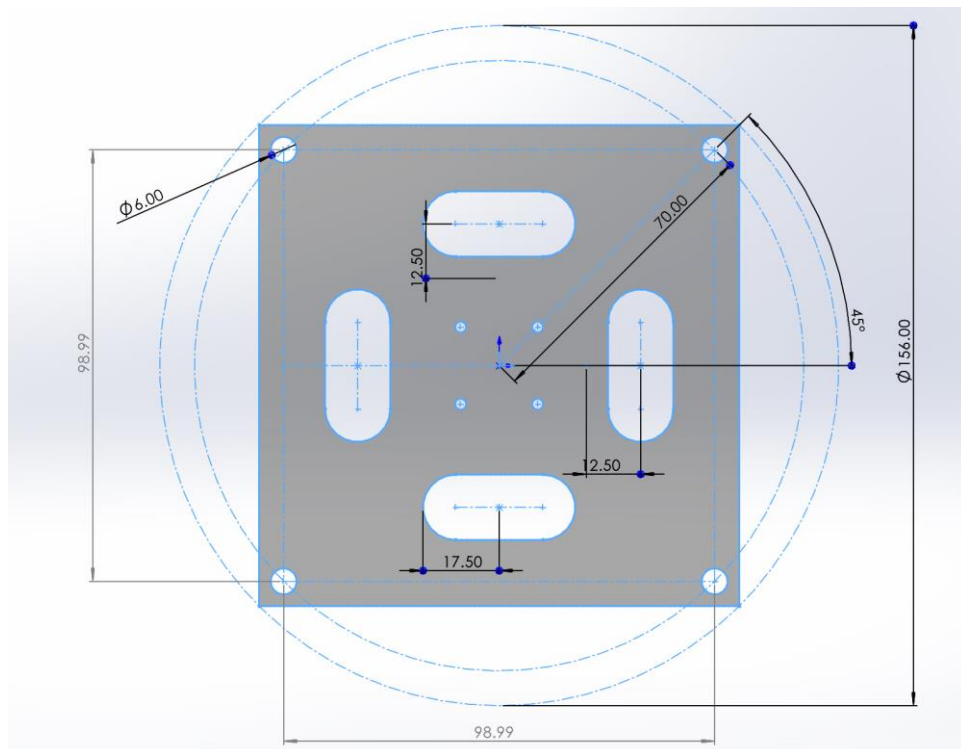
Figure 3-10 - Motor Base with measurements.

To attach the base to the main screws extending from the robot, an initial hole (diameter = 6 mm) was designed at a 45-degree angle from the horizontal, with 70 mm from the centre of the base. The remaining three holes were placed at the corners of a square with sides measuring 98.99 mm.

3.3.4   Inertia

The formula that relates the robot's rotation time for a specific angle with the motor's speed is given by:

$$I_{rw} \cdot \omega_{motor} = 2 \cdot I_{robot} \cdot \frac{\theta}{t_{rot}} \qquad (3\text{-}5)$$

Where:

- I_{rw}, is the inertia of the reaction wheel, including both the rotor and the wheel,

- ω_{motor}, is the angular velocity of the motor,

- I_{robot}, is the inertia of the robot about its vertical axis,

- θ, is the desired rotation angle of the robot,

- t_{rot}, is the desired time for the robot to complete the rotation.

The total inertia of the reaction wheel is the sum of the inertias of the wheel and the rotor. The inertia of the wheel can be estimated using SolidWorks (as shown in Table 3-2), where I_z represents the inertia along the vertical axis, which aligns with the robot's axis of rotation. For the rotor, since the value is not in the datasheet, it can be estimated using equation (3-6) if the mass (M) and radius (R) are known. However, these values are not specified in the datasheet. Given that the total mass of the motor is 64 g, it is assumed that the rotor's mass constitutes only a fraction of this, therefore the rotor's inertia can be neglected.

Axis	Inertia
I_x	$0.00135 \; kg/m^2$
I_y	$0.00135 \; kg/m^2$
I_z	$0.00254 \; kg/m^2$

Table 3-2 - Inertia Measurements of Wheel

$$I = \frac{1}{2} \cdot M \cdot R^2 \qquad (3\text{-}6)$$

Using equation (3-5), and knowing the inertia of both the wheel and the robot, the maximum angular velocity of the motor required to rotate the robot 360 degrees (2π radians) in 5 seconds can

be calculated as follows:

$$\omega_{motor} = 2 \cdot \frac{I_{robot}}{I_{rw}} \cdot \frac{\theta}{t_{rot}} = 2 \cdot \frac{0.0511}{0.00254} \cdot \frac{2\pi}{5} = 50.54 \; {rad}/{s} \qquad (3\text{-}7)$$

This angular velocity, equivalent to 483 RPM, is well within the capabilities of the motor.

The wheel was intentionally designed with a higher inertia than required to adapt to future projects where additional components may be added to the robot.

3.4   Summary

The chapter provided a detailed explanation of the design and implementation of the reaction wheel system within the air-bearing floating robot. The CAD model, developed in SolidWorks, was used not only to calculate the moments of inertia for both the robot and the reaction wheel system, but also to manufacture the wheel from 316L stainless steel, and any other components needed, such as the motor base. The spoke structure design of the wheel intentionally reduce weight and maximize the moment of inertia. Driving this wheel is the GM3506 BLDC motor, selected for its better controllability and performance over traditional brushed DC motors, drives the wheel. The entire Attitude Control System was centred to the robot's horizontal plane and aligned with its vertical axis. Finally, a pair of counterweights was added to shift the centre of mass to the geometrical centre of the robot.

4 ROBOT ATTITUDE DYNAMICS AND CONTROL VIA RE-ACTION WHEEL

4.1 Introduction

Attitude determination and control is one of the main subsystems in spacecraft. This chapter examines the principles of attitude control for a floating robot, which simulates a spacecraft, using reaction wheels. Reaction wheels allow to control precise control of orientation, without the need for external thrusters, following the principle of conservation of angular momentum, as discussed in Section 2.3.

Moreover, the use of system coordinates is important for attitude determination. The movement of satellites can be described in different frames, so it is important to clearly define each frame, and the transformation matrices needed to transition between them. This chapter introduces the concepts of inertial and rotational frames, along with the various coordinates systems used to describe the robot's orientation.

Additionally, the chapter covers the mathematical modelling of the robot's dynamic behaviour, including the equations of motion and the reaction wheel model. The control theory required to manage the robot's orientation, and the approach used to verify the performance of the control system, are also discussed in detail.

4.2 Coordinate Frames

This section discusses the coordinate frames used to define the motion and orientation of the air-bearing floating robot and its subsystems. The primary frames considered are the Granite Table Frame, the Robot's Body Frame and the Orbit Frame. Additionally, a Mechanical Frame derived from the CAD model is used to transfer coordinates between the body frame and the secondary frames of the robot, including those for the reaction wheel, sensors and Raspberry Pi.

4.2.1 Inertial Frame vs Rotational Frame

In orbital mechanics, the absolute acceleration $\vec{a}$ of an object's centre of mass can be measured within a reference or inertial frame. This reference frame "has neither translational nor rotational acceleration relative to fixed stars" [18] and is governed by Newton's first law, which states that an object will remain in its state of motion unless acted upon by an external force. Typically, the inertial reference frame is usually defined relative to fixed stars or the Earth, but for this project, it is is aligned with the granite table.

Alternately, the rotational frame does accelerate and rotates relative to the inertial frame. In this reference fictitious forces appear, such as centrifugal and Coriolis forces [19]. The Transport theorem links the time derivatives of vectors in rotating and inertial frames and describes how the rotation of

the frame influences the observed motion of the system.

4.2.2 Table Frame

The Table Frame functions as the inertial reference for this project. This frame is fixed to the granite table on which the robot moves. The X-axis aligns with the shorter side of the table, the Y-axis with the longer side, and the Z-axis points upward, completing the coordinate triad. The origin of this frame is set at the lower left corner of the table.

4.2.3 Body Frame

The body frame is a rotating reference frame attached to the robot and aligned to the robot's centre of mass aligned to its principal axis of inertia. This frame describes the robot's dynamics, as the robot moves, the axes on the horizontal plane of this frame rotate around the vertical axis, following the robot's orientation.

4.2.4 Orbit Frame

The orbit frame describes the trajectory of the robot as it moves over the table. This frame tracks the robot's path, with its origin is at the robot's centre of mass. The Z-axis aligned with the table's Z-axis and the Y-axis aligned with the direction of the robot's velocity.

These coordinate frames and their transformations are useful to analyse and control the robot's movement and orientation with respect to the granite table. For a more detailed explanation of these primary frames as well as the secondary frames associated with the reaction wheel, sensors and CAD reference frame please refer to "APPENDIX A: Coordinate System Definition (CSD) Document".

4.3 Robot Kinematics Equations – Passive Control of Reaction Wheel

Assuming the robot has no translational motion, the angular velocity vector of the robot (body) frame relative to the table (inertial) frame can be denoted as:

$$\boldsymbol{\omega}_{b/i} = p\hat{\boldsymbol{i}} + q\hat{\boldsymbol{j}} + r\hat{\boldsymbol{k}} \tag{4-1}$$

For this project the only rotation is about the vertical axis of the robot, a rotation matrix is R_ϕ implemented to describe the rotation over the X-axis of the robot. Since the vertical axis of the robot (X-axis), is aligned to the Z-axis of the table, an extra -90-degrees rotation matrix R_θ has to be added to transformation from the body frame to the inertial frame, see equation (4-2).

$$R_{\phi\theta} = \begin{bmatrix} \cos\theta & 0 & \sin\theta \\ 0 & 1 & 0 \\ -\sin\theta & 0 & \cos\theta \end{bmatrix} \begin{bmatrix} 1 & 0 & 0 \\ 0 & \cos\phi & -\sin\phi \\ 0 & \sin\phi & \cos\phi \end{bmatrix} \tag{4-2}$$

The angular velocity $\boldsymbol{\omega}_{b/i}$ of the body with respect to the inertial frame is then calculated with equation below:

$$\begin{bmatrix} p \\ q \\ r \end{bmatrix} = \begin{bmatrix} \cos\theta & 0 & \sin\theta \\ 0 & 1 & 0 \\ -\sin\theta & 0 & \cos\theta \end{bmatrix} \begin{bmatrix} 1 & 0 & 0 \\ 0 & \cos\phi & -\sin\phi \\ 0 & \sin\phi & \cos\phi \end{bmatrix} \begin{bmatrix} \dot{\phi} \\ 0 \\ 0 \end{bmatrix} \tag{4-3}$$

Substituting $\theta = 90$ degrees in equation (4-3) we can deduce that:

$$\begin{bmatrix} p \\ q \\ r \end{bmatrix} = \begin{bmatrix} 0 \\ 0 \\ \dot{\phi} \end{bmatrix} \tag{4-4}$$

This simplifies the equations as the model can be described only using a single angular velocity:

$$\dot{\phi} = r = \omega \tag{4-5}$$

From the Euler's Moment Equations (**2.6**), applied to a single rotation the rate of change of the angular momentum of the robot can be defined as:

$$\tau = \dot{\omega} \cdot J_b \tag{4-6}$$

Where, $J_b = 0.0511 \; kg/m^2$ is the moment of inertia on the vertical axis of the robot.

The state vector x and control variable are defined by:

$$x = \begin{bmatrix} \phi \\ \omega \end{bmatrix} \tag{4-7}$$

$$u = [\tau] \tag{4-8}$$

Since through the camera and the IMU the position and the angular velocity can be measured, from equations (**2.7**) and (**2.8**) we can deduce the matrix A, B and C for the state $\dot{x} = [\dot{\phi} \quad \dot{\omega}]^T$:

$$A = \begin{bmatrix} 0 & 1 \\ 0 & 0 \end{bmatrix} \tag{4-9}$$

$$B = \begin{bmatrix} 0 \\ 1/J_b \end{bmatrix} \tag{4-10}$$

$$C = \begin{bmatrix} 1 & 0 \\ 0 & 1 \end{bmatrix} \tag{4-11}$$

4.3.1 Controllability of Outer Loop

From equation (**2.9**) the controllability matrix (Q_c) can be calculated:

$$Q_c = \begin{bmatrix} 0 & 19.5465 \\ 19.5465 & 0 \end{bmatrix} \tag{4-12}$$

Because the rank of Q_c, -rank(Q_c) = 2-, is equal to the size of the matrix A from (4-9), the system is considered as fully controllable.

4.3.2   Observability of Outer Loop

Similarly, because the rank of the observability matrix, Q_o, calculated from equation(**2.10**), is equal to the size of the matrix A; the system is fully observable.

$$Q_o = \begin{bmatrix} 1 & 0 \\ 0 & 1 \\ 0 & 1 \\ 0 & 0 \end{bmatrix} \tag{4-13}$$

The controllability and observability matrices and ranks can be calculated using the MATLAB commands "*ctrb(A, B);*" and "*obsv(A,C);*"; refer to APPENDIX B: MATLAB Scripts.

The transfer function for the orientation of the satellite, obtained from the state-space representation is:

$$\frac{\phi}{\tau} = \frac{1}{J_b \cdot s} \tag{4.14}$$

4.4   Control Torque with Reaction Wheels in Passive Mode

Once it is stated that the system is controllable and observable, the open-loop poles of the system can be computed using the determinant in (4-15):

$$p = det(sI - A) \tag{4-15}$$

Then, using the state feedback controller strategy from (2.4.3) new poles can be determined to stabilize the system for a required time response in closed loop. The values of the matrix K are equivalent to a proportional, K_p, and derivative, K_d, gains of a controller of the form:

$$T = K_p(\phi_{err}) + K_d\dot{\phi} \tag{4-16}$$

The output of the controller is used as the torque reference for the inner loop.

4.5   Reaction Wheel dynamics

4.5.1   Motor Electrical & Mechanical Equations

Given the three-phase nature of a BLDC motor, equations that describe the model turn complex, as shown below:

$$V_a = R_a I_a + L_a \frac{di_a}{dt} + M_{ac}\frac{di_b}{dt} + M_{bc}\frac{di_c}{dt} + e_a,$$

$$V_b = R_b I_b + L_b \frac{di_b}{dt} + M_{ac}\frac{di_a}{dt} + M_{bc}\frac{di_c}{dt} + e_b, \tag{4-17}$$

$$V_c = R_c I_c + L_c \frac{di_c}{dt} + M_{ac}\frac{di_b}{dt} + M_{bc}\frac{di_c}{dt} + e_c,$$

where V_a, V_b, and V_c are the stator phase voltages; R is the resistance per phase, i_a, i_b and i_c are the

stator phase currents; $L_a = L_b = L_c$ are the self-inductances of each phase, and are considered equal and constant for each phase. M_{ac} and M_{bc} are the mutual inductances and e_a, e_b and e_c are the back electromotive forces. The Back EMF is trapezoidal and is a function of the rotor speed ω, and position θ:

$$e_a = f_a(\theta)\lambda\omega,$$

$$e_b = f_b(\theta)\lambda\omega, \qquad (4\text{-}18)$$

$$e_c = f_c(\theta)\lambda\omega,$$

where λ, is the total flux linkage. The total electromotive torque T_e, in [Nm] can be represented as a function of all phases:

$$T_e = \frac{e_a I_a + e_b I_b + e_c I_c}{\omega}. \qquad (4\text{-}19)$$

Or by:

$$T_e - T_L = J\frac{d\omega_m}{dt} + B\omega_m. \qquad (4\text{-}20)$$

However, this type of model requires to adapt an extra three-phase invertor, which complicates modelling the plant. An C.O.T.S. Electronic Speed Controller, (ESC), which applies a Sensorless Control of BLDC Motors Technique through reading the back-EMF, is used for this the motor model and therefore it can be simplified to a Three constant motor model DC (See Figure 4-1) [21].

4.5.2 Three-Constant motor model DC representation

In literature there exist several models of BLDC motors, but one of the most common is the Three-Constant BLDC motor model, which is a normal DC representation of the brushless motor, using only three of its parameters.
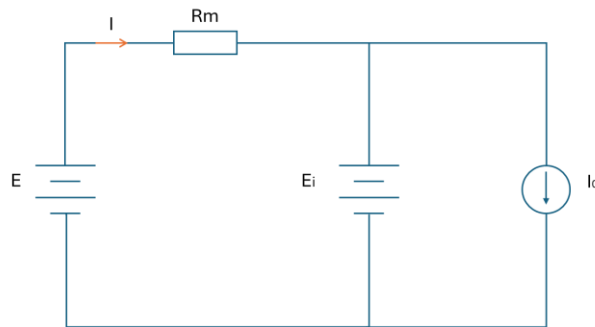

Figure 4-1 – Three-constant motor model DC representation of a three-phase motor.

The three constants are the speed constant K_V, the motor resistance R_m, and the no load current I_0. Alternately to the speed constant, some authors use the torque constant K_t. Inductances are not used in this model as the dynamics of the electronic part of the loop is much faster than the

electromechanical dynamics. In general, the electronic part settles approximately ten times faster than the mechanical part.

This model allows to rewrite equations (4-25), (4-27) and (4-20) as:

$$e = K_e\omega, \tag{4-21}$$

$$E = V = Ri + K_e\omega, \tag{4-22}$$

$$T = K_t i, \tag{4-23}$$

$$J\dot{\omega} + b\omega = K_t i, \tag{4-24}$$

where Ke=Kt. Considering that ω is the angular velocity of the wheel with respect of the satellite, plant can be modelled on block diagram, as in Figure 4-2 and the transfer function that takes the rate of change of the angular momentum as a function of the input voltages can be calculated.
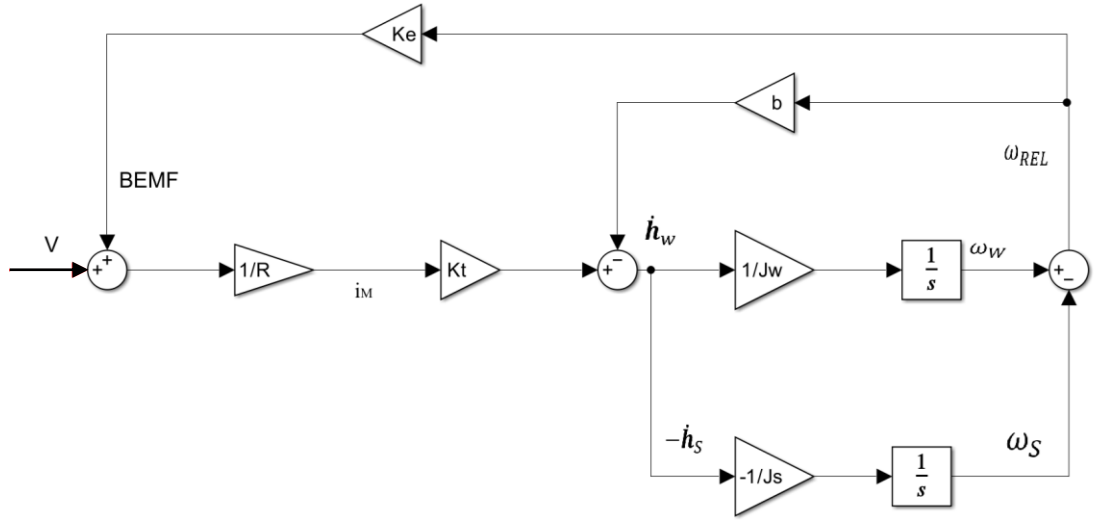
Figure 4-2 - Momentum exchange devise model.

Figure 4-2 denotes the basic model of a moment exchange device, J_w and J_s are the moment of inertia of the reaction wheel and the spacecraft, in this case the robot. ω_{REL} is the angular velocity of the reaction wheel relative to the robot and b is the damping friction coefficient. In this model V is the input voltage of the motor.

Since no external disturbances, T_d, are affecting the system, the main relation between the reaction wheel and a satellite, or in this case the robot, is defined by the Euler's moment equation of angular motion:

$$\dot{h}_S + \dot{h}_w = 0 \tag{4-25}$$

To apply a torque on the body, the motor must produce a torque in the opposite direction:

$$\dot{h}_S = -\dot{h}_w \tag{4-26}$$

Therefore, from Figure 4-2 and equations (4-25) and (4-26) the transfer function that relates the rate of change of the angular momentum of the reaction wheel, and the voltage of the motor can be

defined as:

$$\frac{\dot{h}_w}{V} = \frac{I_w \dot{\omega}_w}{V} = \frac{s\left(\frac{K_M}{R_M}\right)}{s + \left(\frac{1}{I_w} + \frac{1}{I_S}\right)\left(\frac{K_V K_M}{R_M} + B\right)} \tag{4-27}$$

The output of equation above is the rate of change of the angular momentum, equivalent to the torque. However, the input from the outer controller is also torque so the transfer function from (4-27) must be updated converting the torque $\dot{h}_w$ a response of a command T_c. Figure 4-3 shows the block diagram of a reaction wheel in torque mode [5].
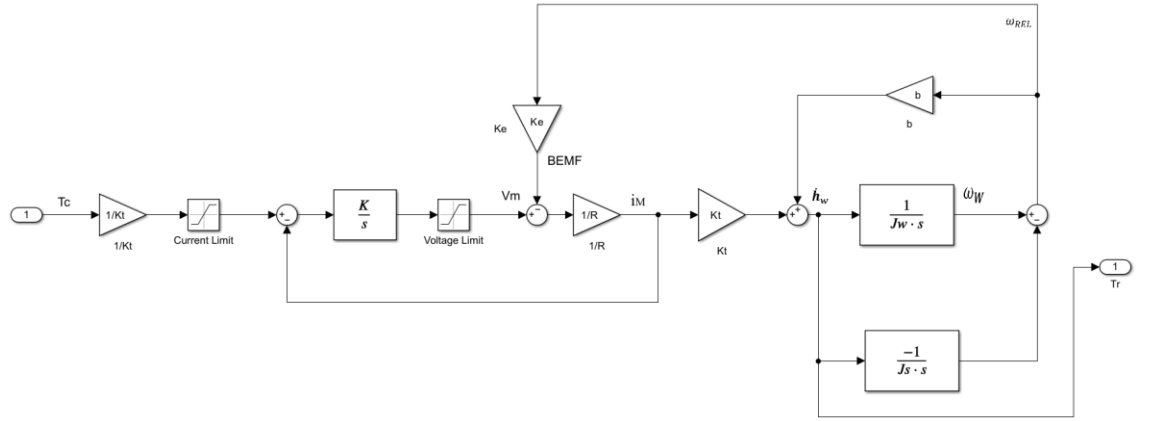
Figure 4-3 - Reaction Wheel in torque mode.

Additionally, it is possible to neglect the viscosity damping coefficient, b, as it is several orders of magnitude smaller than the other variables. Considering also that the inertia of the Robot is more than 20 times bigger than the one from the wheel, the modified transfer function that relates the commanded and reaction torques, with an integral gain to control the voltage according to a desired torque, according to Figure 4-3:

$$\frac{T_r}{T_c} = \frac{\dot{h}_w}{T_c} = \frac{K/s \cdot R}{1 + \frac{K}{s \cdot R}\left(1 + \frac{K_e \cdot K_t}{K \cdot J_w}\right)} \tag{4-28}$$

Notice that Figure 4-3 adds a feedback path from the motor current, as it is proportional to the electrical torque produced by the motor. A gain K, is also added before the voltage input. If that gain K, is set that

$$K \gg \frac{K_e \cdot K_t}{J_w} \tag{4-29}$$

So that the term in the parenthesis at equation (4-28) has a value of ~1. Equation (4-28) can then be rewritten as in (4-30), a first-order equation with a time constant depending on the resistance of

the motor.

$$\frac{\dot{h}_w}{T_c} = \frac{1}{1 + s(R/K)} \tag{4-30}$$

From the simplified transfer function, it was verified that the system is observable and controllable through a state-space representation using MATLAB.

4.6   Summary of Mathematical Developments

This chapter provided a detailed description of the kinematic and dynamic equations for attitude control using reaction wheels. It demonstrated how the relationships between various reference frames—such as the body and inertial frames—can be mathematically manipulated to measure and control the robot's angular velocity. The use of transformation matrices between these frames was essential in defining the robot's orientation and movement.

Additionally, important control concepts like observability, and controllability, were introduced for the passive attitude control system. The chapter explained how control strategies, such as full-state feedback and pole placement, were applied to stabilize the system in a closed-loop configuration. The analysis of the system's step response and pole locations helped to obtain the gains for the correct control of the system.

A simplified model of reaction wheels driven by brushless motors was also discussed, demonstrating their effectiveness in stabilizing the system. In conclusion, reaction wheels, combined with appropriate mathematical models and control strategies, provided the necessary stability and precision for controlling the robot's orientation.

5   NUMERICAL SIMULATIONS IN SIMULINK

5.1   Introduction

This chapter presents the simulations conducted in Simulink and MATLAB to validate the control design for the reaction wheel system of the air-bearing floating robot. The control architecture includes both an inner and an outer loop, where the inner loop focuses on controlling the reaction wheel's torque and the outer loop controls the robot's attitude. The simulations evaluate the system's response to different inputs, ensuring that the desired orientation is achieved while considering the physical limitations of the motor, such as maximum torque and angular velocity.

Through a tuning process of the controller gains (K_p and K_p), the behaviour of the system can be improved to minimize overshoot, reduce settling time, and ensure a smooth and stable response. The chapter explores various pole placements and optimization technique, discussed in the previous chapter, and compares different sets of gains to achieve optimal performance. The effectiveness of the

controller is analysed through step responses of the system, along with the torque and angular velocity responses of both the reaction wheel and the robot. These simulations show how the system behaves under different scenarios and how control parameters can be adjusted to meet the project's requirements. All Simulink Models can be found in APPENDIX B: MATLAB Scripts & Simulink Models.

5.2   Simulink Models

5.2.1   Outer Loop

Through some block algebra, the block representation of the outer loop, based on Figure 2-2, is modelled in Figure 5-1. Here, K_p and K_d correspond to the values from the torque control (4-16). The open loop has both poles at zero (5-1). This indicates that the system behaves as a double integrator, which means it is marginally stable. While it does not diverge exponentially, a constant input will make the output grow indefinitely (see Figure 5-2).

$$s_{1,2} = 0 \tag{5-1}$$
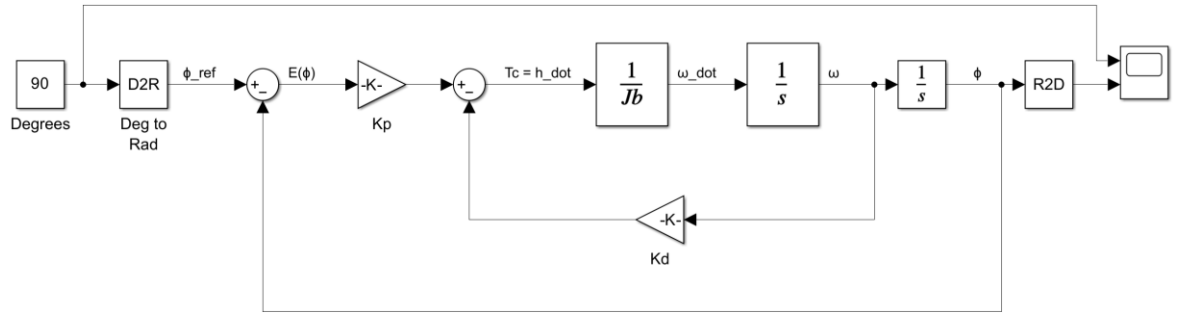
Figure 5-1 - Outer Loop - Robot Attitude Control
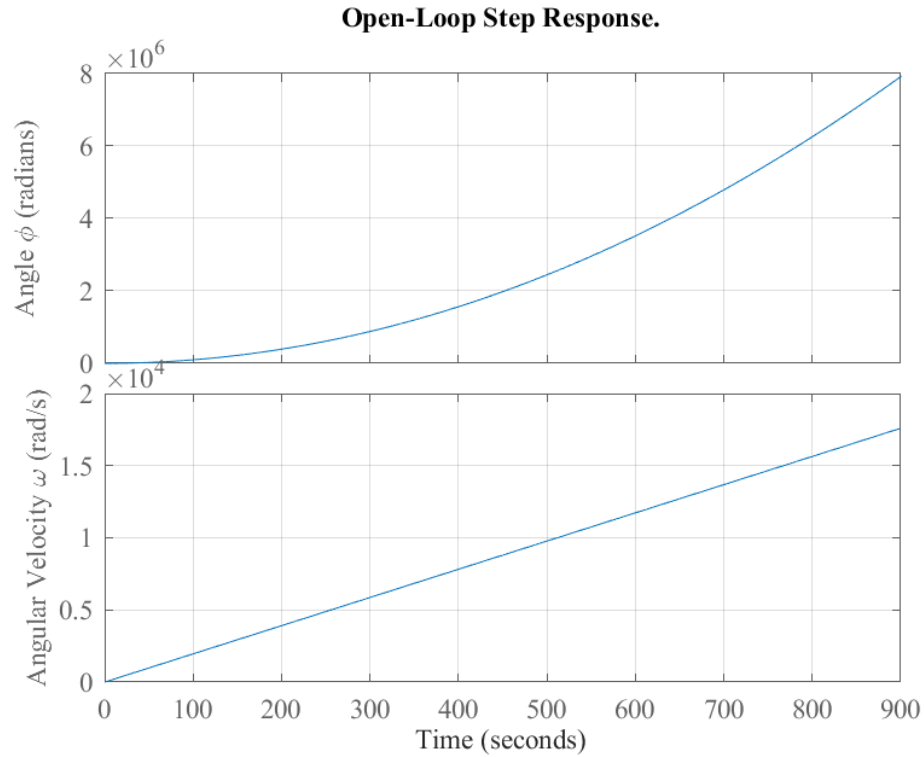
Figure 5-2 - Open-Loop Step Response of Attitude Control

Different pole pairs were tested. Although poles placed farther from the imaginary axis achieve faster response times [20], the desired real poles were chosen not far from the axis, to prevent the system from significantly lowering its steady-state gain. Figure 5-3 shows the step response for different pole pairs. For each pair of poles, a matrix K was computed using a MATLAB script (APPENDIX B: MATLAB Scripts).

The new poles selected for the system (see Figure 5-4), through optimization where:

$$p = [-4.89, -3.998] \tag{5-2}$$
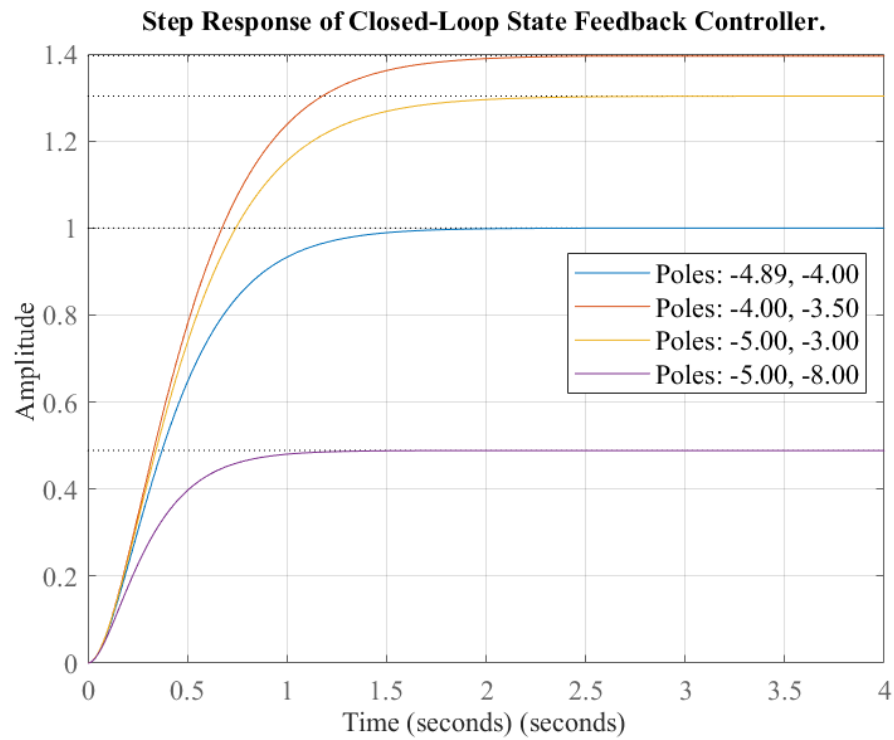
Figure 5-3 - Step Response for different Poles.
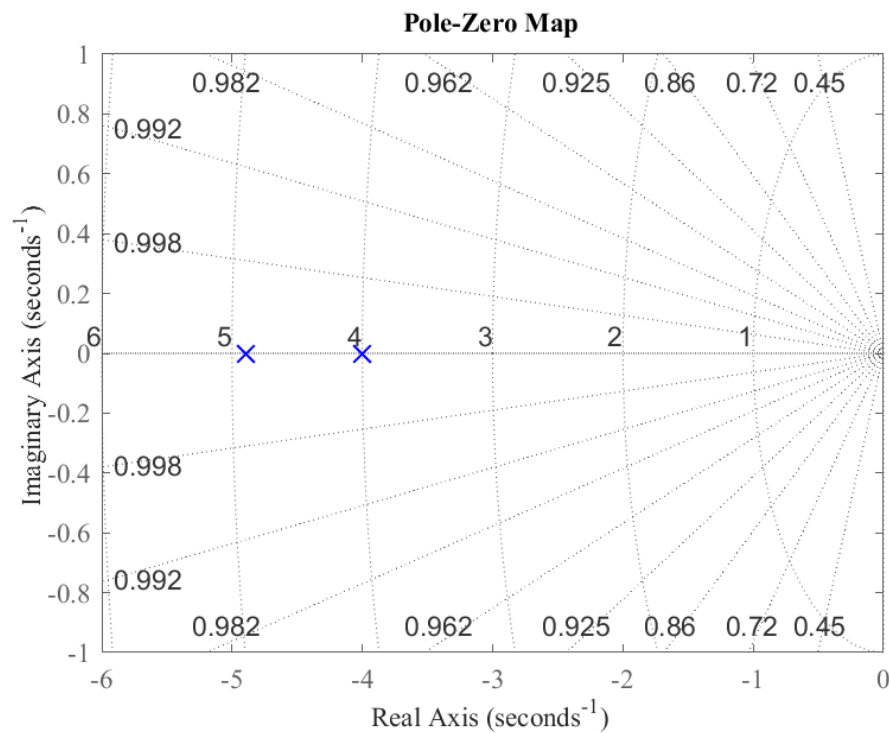
Figure 5-4 – Poles location using Full-State Feedback Control, P1(-4.89,0), P2(-3.998,0).

The matrix K that stabilizes the system with these poles is defined as follows:

$$K = [1.0002 \quad 0.4547]$$ (5-3)

Figure 5-5 shows the response for orientation and angular velocity based on the selected poles.
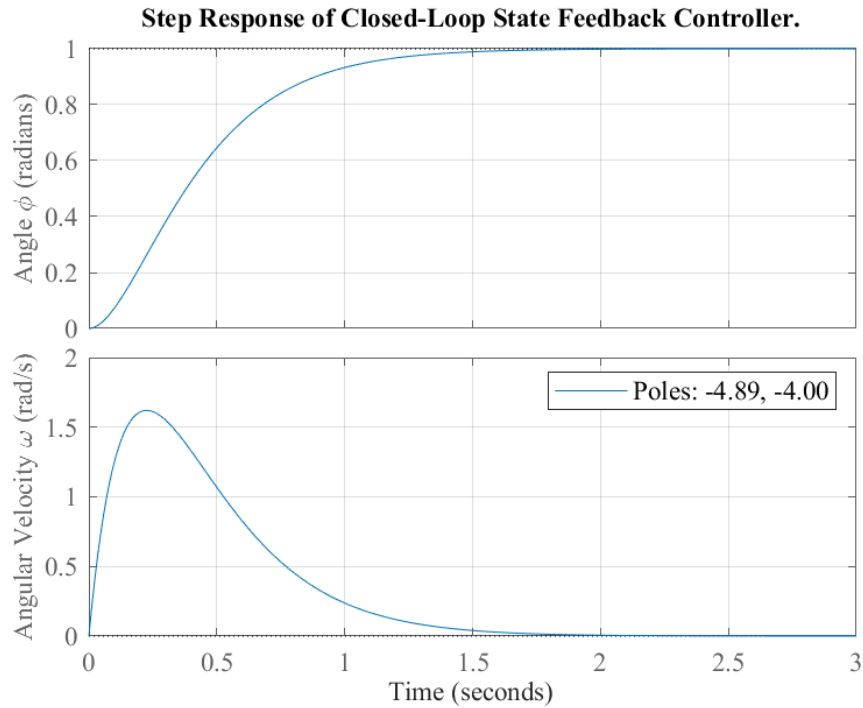
Figure 5-5 - Closed Loop Step Response of State Feedback Controller.

5.2.2 Inner Loop

Figure 5-6 shows the simplified model of a reaction wheel based on the transfer function derived in Equation (4-30). The torque limit is set to 80% the maximum torque provided by the motor to prevent saturation. However, this limit can be adjusted to ensure the motor operates within safe torque limits. The Gain K is calculated by substituting Equation (4-29) with the parameters from Table 5-1, the gain then should have a value higher than 1.7938.
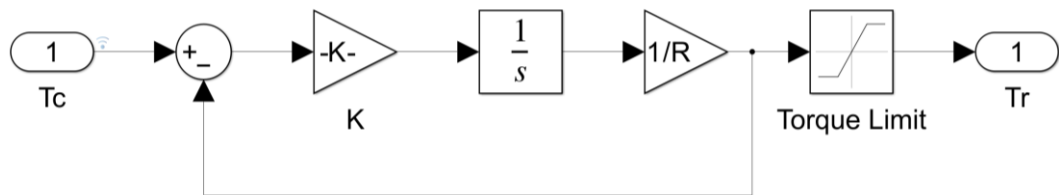
Figure 5-6 -Simplified Torque Mode of a Reaction Wheel.

Parameter	Value	Unit
Ke	0.06754	V*s/rad
Kt	0.06754	Nm/A
R	5.6	Ohms
Jw	0.00254	Kg*m^2
Js	0.05116	Kg*m^2

Table 5-1 – Reaction Wheel Mechanical Parameters

The inner loop must be at least ten times faster than the outer loop, so that the outer loop gains calculated from the passive control of the reaction wheel could be valid in an active control of the wheel. The K value was chosen, through Simulink, to achieve a settling time of $T_s = 0.001\ s$, with an undershoot of $Q \leq 5\%$. The resultant value of K and the parameters for the step response are shown in Table 5-2. Figure 5-7 presents the step response of the plant. The farther location of the pole from the imaginary axis, at $p = -2000$ as shown in Figure 5-8, confirms the faster response of the motor system,

Parameter	Value
Gain **K**	11200
Rise Time	0.0011 seconds
Settling Time	0.00196 seconds
Overshoot	0 %

Table 5-2 - Step Response Parameters for K=11200.
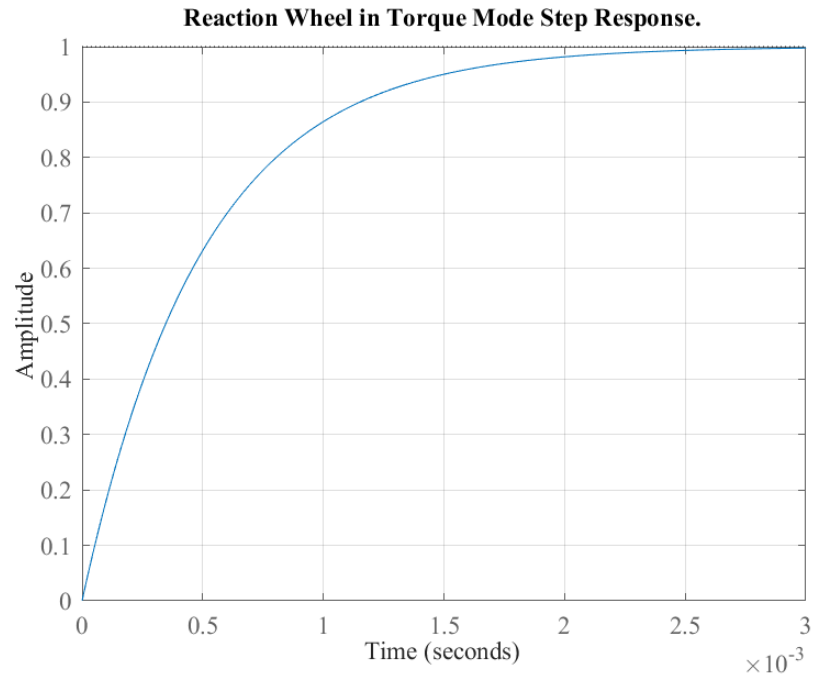
Figure 5-7 - Step Response of Simplified Torque Mode Reaction Wheel without limited Torque.
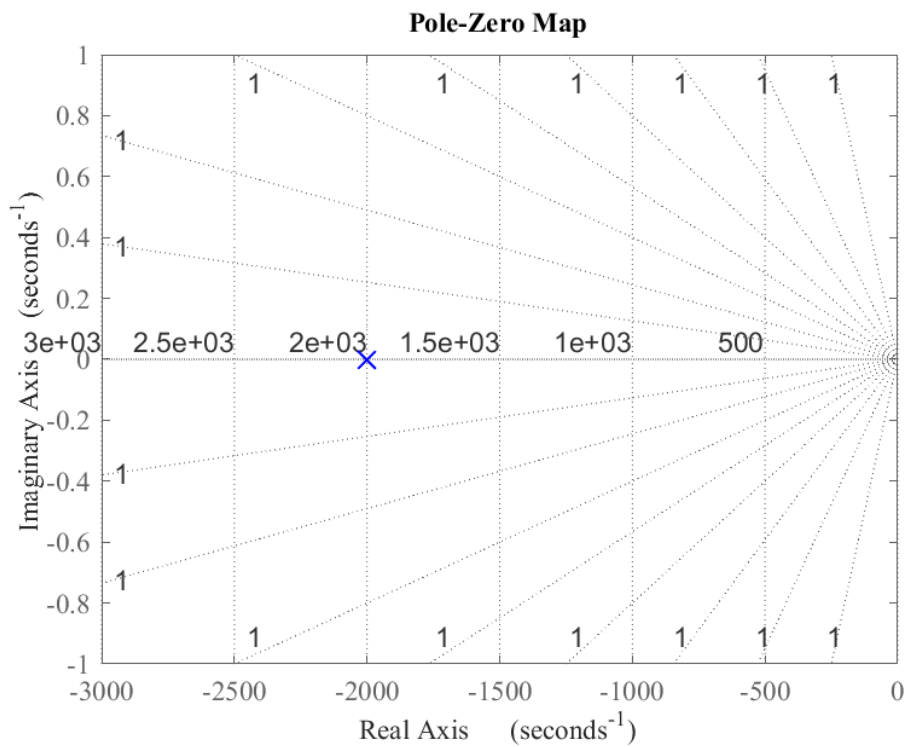
Figure 5-8 - Pole location of Reaction Wheel System.

5.3 Numerical Experiments

In complete control loop is showed in Figure 5-9, the simplified mode corresponds to the reaction wheel inner loop. The control law works perfectly for small angles, where $\varphi \approx 0$, see Figure 5-10, making it ideal for stabilization due to the simplicity of the equations. However, for large manoeuvres, due to the motor's physical limitations (voltage, current, torque, etc…), the response overshoot increases. The Feedback Controller does not account for these limitations. To address this, the first solution was to bound the angle setpoint to $-180\ deg \leq \varphi \leq 180\ deg$, as the objective is to rotate the robot to a desired orientation, not to perform continuous rotations. However, for higher setpoints, for example 170 degrees, a ~27% overshoot was observed (Figure 5-11). Through further optimization, new values for K_p and K_d were obtained for the matrix K:

$$K = [0.9 \quad 1] \tag{5-4}$$
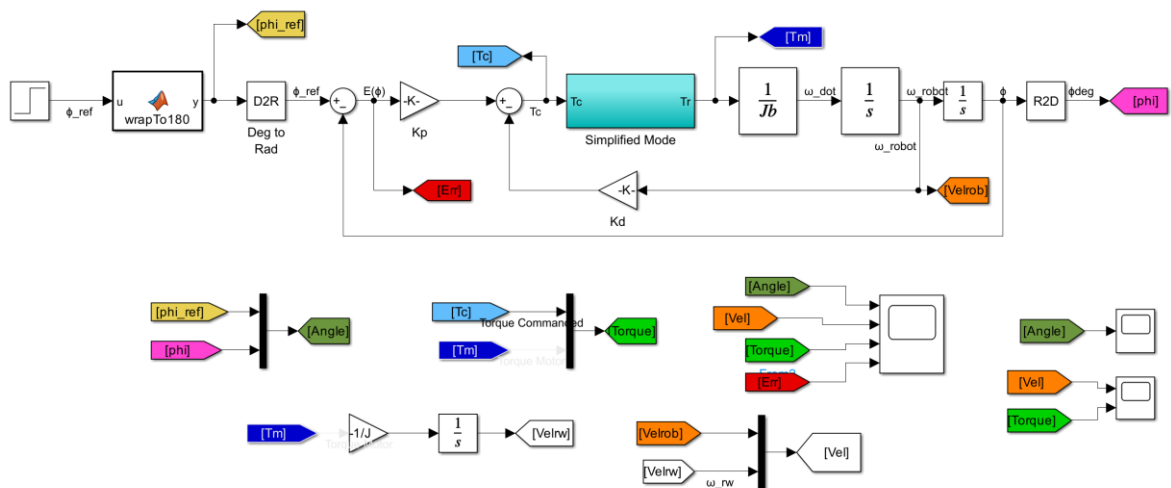
Figure 5-9 - Complete Robot Attitude Controller.

Figure 5-10 – Step response of amplitude 10-degrees. Gains: Kp = 1.0002, Kd = 04547 .
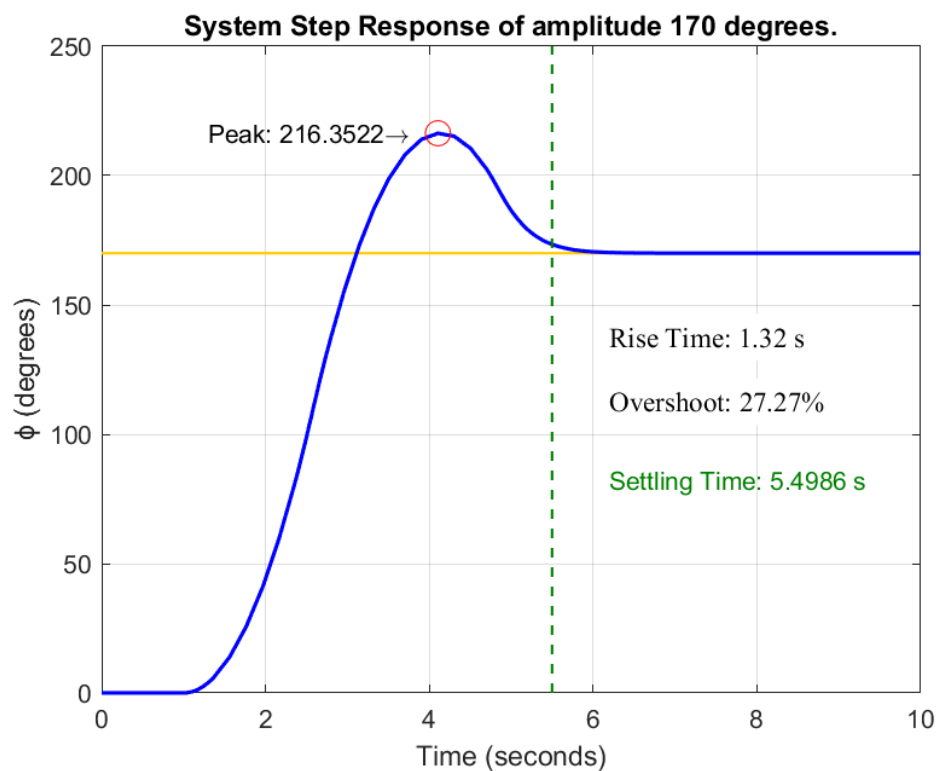
Figure 5-11 - Step response for a 170-degrees step. Gains Kp = 1.0002, Kd = 04547.

Figure 5-12 shows the system's angular velocity and torque responses with the updated controller gains $K_p = 0.9$ and $K_d = 1$. The reaction wheel rotates faster initially to generate the necessary

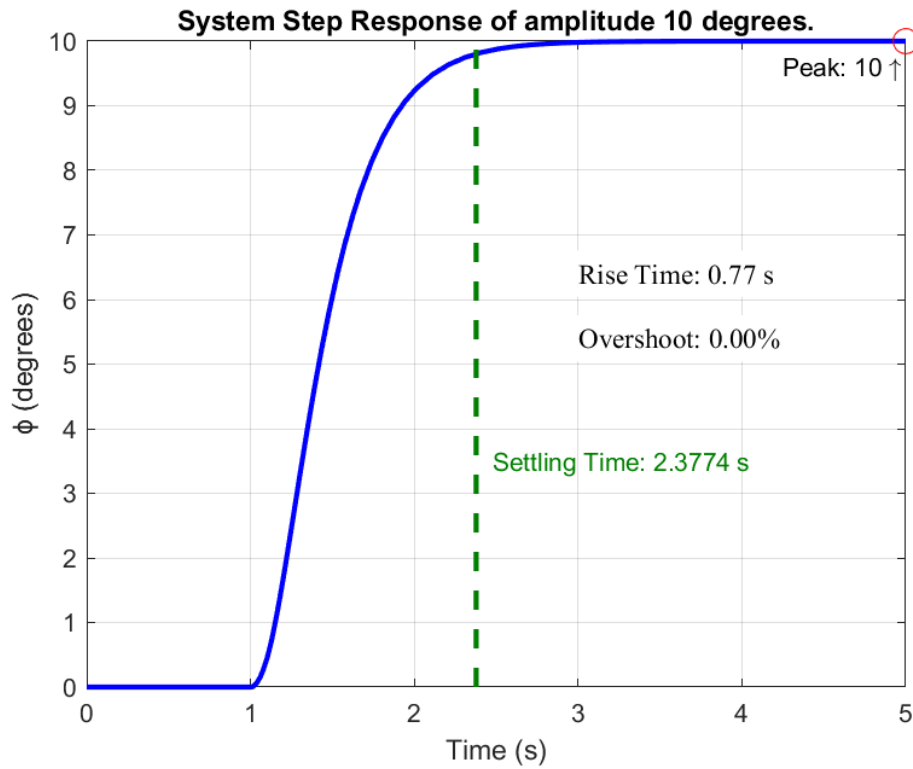torque to rotate the robot to the desired orientation. In the bottom graph, the blue line represents the torque commanded by the outer loop controller, while the orange line shows the torque produced by the reaction wheel. The actual torque output is significantly lower due to the physical limitations of the motor. The motor reaches its maximum torque capacity and remains saturated for a brief period, as seen in the plot. It is important to note that, although the torque commanded, and the torque generated by the reaction wheel are opposite in nature, the reaction torque plotted is the rate of change of the angular momentum of the robot.
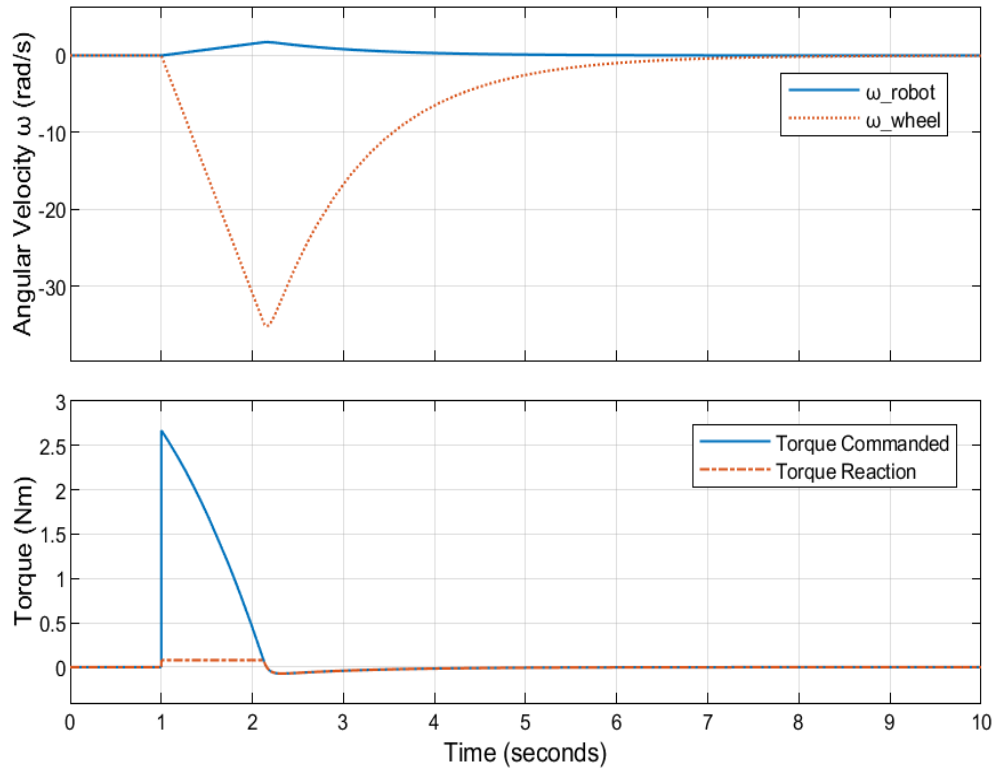
Figure 5-12 – Top: Comparison between the angular velocity of the robot and the reaction wheel. Bottom: Commanded torque vs actual torque reaction of the robot.

Although, the updated controller gains $K_p = 0.9$ and $K_d = 1$ result in a slower system response (Figure 5-13), with a settling time of 5.8 seconds, the response is noticeably smoother compared to previous configurations. The system now exhibits a rise time of 2.53 seconds and, mor importantly, no overshoot, which indicates improved stability. This smooth response confirms that the system reaches the desired setpoint without exceeding it. While the response is slower, the absence of oscillations and overshoot demonstrates the trade-off made between speed and stability. The updated gains result in a well-controlled response that is more appropriate for the sensitive manoeuvres required by the reaction wheel system.
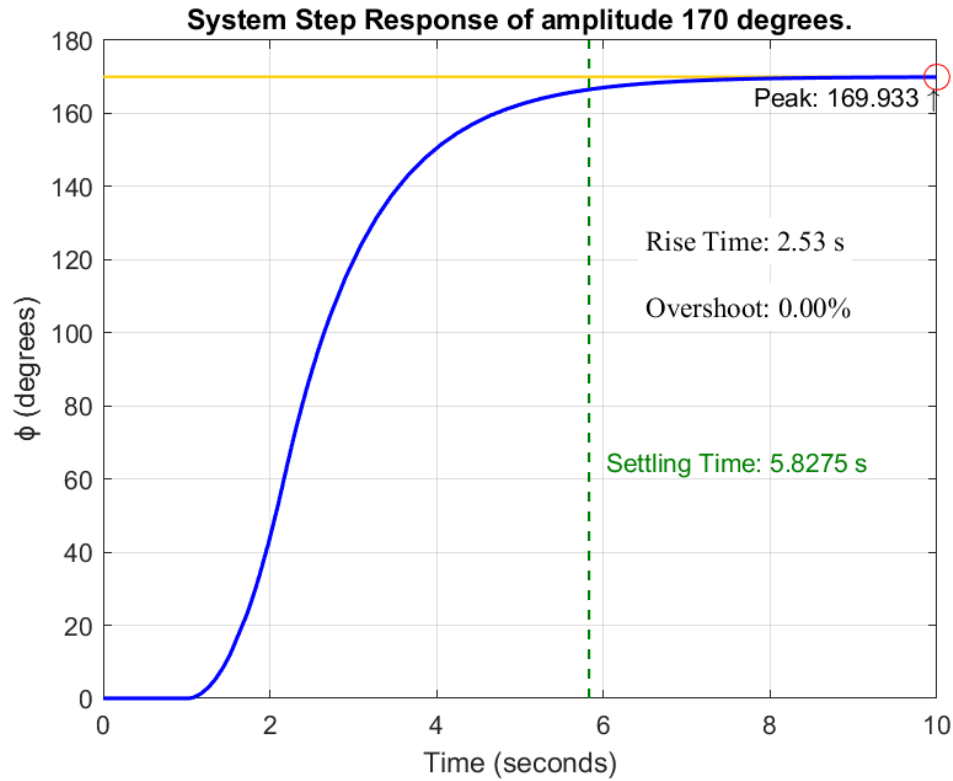
Figure 5-13 – Plant Step response of amplitude 170 (deg.). Gains Kp = 0.9 & Kd = 1.

5.4   Summary

In this chapter, the reaction wheel system's numerical simulations were performed to evaluate its performance in rotating a floating robot. Different control strategies were tested, and controller gains were adjusted to improve the system's response to step inputs. The results indicate that while the initial configuration of gains, calculated through a feedback controller strategy that did not consider the mechanical limitations of the motor and assumed passive control of the reaction wheel, produced overshoot and oscillations when implementing an active control, the optimized gains of $K_p = 0.9$ and $K_d = 1$ provided a more stable and smoother response. The system reached the desired orientation without overshooting, and although the settling time was slightly longer, it was still in an acceptable range. However, the reaction wheel's torque was limited by the motor's mechanical and electrical constraints, but the latter simulations considered these limitations.

The results demonstrate the effectiveness of the full-state feedback control even when considering the passive behaviour of the reaction wheel. Nevertheless, extra tuning had to be performed to account for the system's physical limitations. By adjusting carefully the control gains, the system was able to balance the performance and the physical restrictions, leading to a stable, smooth, and efficient attitude control system. These simulations provide a reliable approach for validating control laws applied to the reaction wheel system and ensure that the system can meet operational requirements for future space systems testing.

6 CONCLUSION

This dissertation presents the design and implementation of an Attitude Control system (ACS) using a single-degree-of-freedom Reaction Wheel for an air-bearing floating robot. The system was designed to allow the robot to change its orientation based on a user input, simulating the n microgravity conditions found in space. The project covered various aspects, from mechanical design and CAD modelling to control algorithms and Software-in-the-Loop (SIL) testing, resulting in a system that meets the project's objectives.

The development of the reaction wheel system, which generates enough torque to control the robot's attitude, was a major achievement in this project. The integration with SIL testing allowed for real-time verification and adjustments of the control algorithms, showing that the system could reorientate to a desired angle. Some challenges were encountered, such as hardware limitations and difficulties in tunning the control due to unavailable motor parameters not provided from the manufacturer, but the system still showed stable and accurate results in the simulations.

The CAD process was important to make sure all components fit and worked together within the floating robot, to obtain the robots parameters such as centre of mass location, moments of inertia and weight of the robot. These values were useful for designing the wheel. and for calculating the rotating matrices to convert between different coordinate systems.

The real robot was not symmetric as it had components mounted in different parts of the main frame. As a result, the centre of mass and the principal axes of inertia were not aligned with the geometric centre, which made the robot to rotate in a way that wasn't aligned with its principal axes of inertia. This added complexity to the mathematical modelling of the system. To correct this, counterweights were added to align the motor's axis properly.

The control law was divided into two parts: an outer loop and an inner loop. The two-loop system was used to separate the motor control from the rest of the satellite. The reaction wheel system was treated as an independent subsystem. The outer loop controlled the robot's attitude along one axis and was designed using a full-state feedback controller (pole placement strategy). Initially, the reaction wheel was treated as passive (a gain of 1), and the control law was based on a proportional-derivative equation, $T = K_p(\phi_{err}) - K_d\dot{\phi}$, here the angle error and angular velocity of the robot multiplied by specific gains provided the torque input for the inner loop. However, this strategy did not contemplate the mechanical limitations of the motor plant, making the response to produce an overshoot and to oscillate as the desired angle increased. Further adjustments to the outer loop gains were made considering the motor's physical limitations, such as voltage, current and torque, once the inner loop was designed.

The inner loop simulated the behaviour of the motor, which was a three-phase BLDC motor. Since

the manufacturer did not provide many motor parameters, a simplified three-constant DC model representation was used instead. After determining the transfer function of the system and through some block algebra, an integral gain was calculated to make the system respond like a first-order plant, adjusting the torque based on a commanded input (the control signal from the outer loop). The inner loop needed to respond at least 10 times faster than the outer loop, so the motor's response time was optimized based on settling time and undershoot requirements. In this simulation, the motor's physical limitations, such as voltage, current, and torque, were considered.

In conclusion, this project shows how reaction wheels can be applied to control small satellited and robotic platforms. The work done here shows that the control system is effective in controlling the robot's orientation in a simulated environment. The results open possibilities for future work, such as improving the hardware, upgrade the control strategy to make the robot to reorientate while translating over the table or design different control laws using the full three-phase design of the motor.

6.1 Evaluation

This project aimed to achieve three main objectives, explained in section 1.2, all of which were successfully completed through simulations, despite delays in receiving the physical components. The first objective was to create a detailed CAD design of the air-bearing robot with a Reaction Wheel assembly. The CAD design was done in SolidWorks, and all the necessary components were sized and included following the CubeSat standard of modularization of subsystems to allow for attitude control experiments. This model included, apart from the main robot frame, different components such as a LiPo battery, a Raspberry Pi, an IMU, and a camera module. Even though the wheel was slightly oversized, the motor was still available to spin with the wheel mounted; this will allow future projects to add components to the robot without redesigning the wheel.

The second objective focused on developing a PID controller. This goal was achieved through describing the system mathematically and modelling it in Simulink. It was divided into two loops, the outer loop was designed as a PD controller while the inner loop incorporated and Integral gain to stabilize the plant.

The third objective was for the robot reorient itself based on user-commanded attitude settings. Although initially the objective was to develop the physical system and do physical tests, due to the delays in receiving the components the goal was modified to achieve it in Simulations. In that way, the goal was accomplished as the plant responded accurately to input commands, showing that the system could perform the required attitude adjustments in real life.

In summary, all project goals were met through simulations and CAD modelling, despite the absence of physical testing due to component delays. The simulations allowed to completely validate

the system, showing that the Attitude Control system, worked as expected in a virtual environment.

6.2   Future Work

The next step in this project will involve incorporating the physical components into the existing model and conducting physical tests. This includes integrating the PWM-controlled brushless DC motors. Performing these physical tests will provide a more accurate evaluation of the system's performance and will help to identify any adjustments needed for space applications.

6.2.1   PWM Implementation for BLDC Motors

Implementing a Pulse Width Modulation (PWM) control involves measuring certain parameters from the motor that are not provided by the manufacturer, such as self and mutual inductances, and using a three-phase invertor, or in this case, an Electronic Speed Controller (ESC) unit. The ESC regulates the speed and torque of BLDC motors through PWM by controlling the amount of voltage applied over time. Despite limited documentation on ESC modules, it has been proven that they can achieve performance levels above 95%, making them ideal for this application, where the inner loop needs to be as fast and precise as possible. Another thing to consider is that not all ESC modules are bidirectional and would only control the motor speed on one direction. Figure 6-1 shows a PWM controller of a BLDC motor. Although this controller design was initially proposed, due to the lack of parameters available of the motor and no form of measuring them a simplified DC representation was implemented.
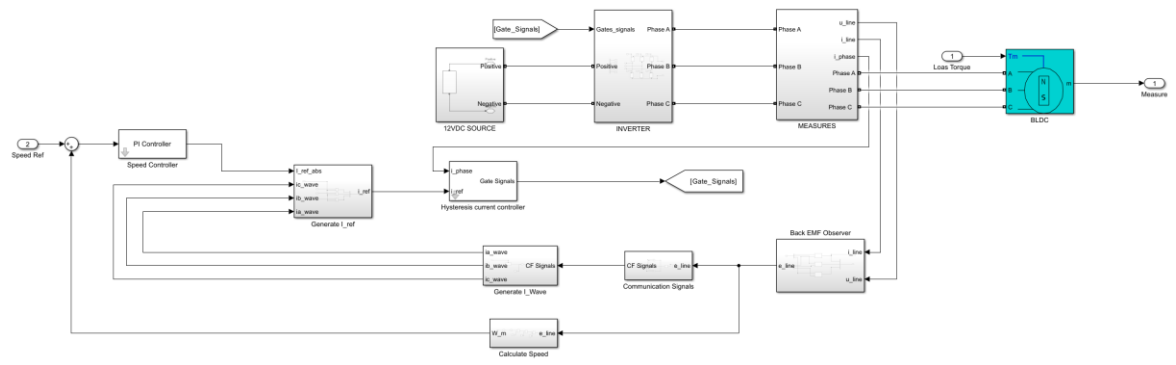
Figure 6-1 - PWM Sensorless Controller of a BLDC motor.

6.2.2   No Body and Axis of Inertia Alignment

Another issue identified is the misalignment between the robot's body and its principal axes of inertia. Since the robot's components are not symmetrically distributed, the centre of mass and the axes of inertia do not align with the geometric centre. This leads to undesired rotational behaviour that complicates the control system. To correct this, counterweights were added to align the robot's principal axis of inertia, with the rest of the frames. However, further work will be needed to study the

effects of this misalignment in real-world conditions, especially once the physical components are fully integrated.

7   REFERENCES

[1] Schwartz, J. L., Peck, M. A., & Hall, C.D. Historical Review of Air-Bearing Spacecraft Simulators, *Journal of Guidance, Control, and Dynamics*, 26(4), 513-522. July-August 2003. DOI: 10.2514/2.5085.

[2] Selection of Electric Motors for Aerospace application, Lesson Number 893. MSFC, NASA Public Lessons Learned System, https://llis.nasa.gov/lesson/893, February 1999.

[3] Rasmussen, R.E. Air Bearing Based Satellite Attitude Dynamics Simulator for Control Software Research and Development, *Calhoun, Institutional Archive of the Naval Postgraduate School*. 2001.

[4] Robotic arm reaching for air-bearing platform. ESA Agency. https://www.esa.int/ESA_Multimedia/Images/2015/12/Robotic_arm_reaching_for_air-bearing_platform, December 2015.

[5] Sidi, M. *Spacecrafts Dynamics & Control: A Practical Engineering Approach*, Cambridge: Cambridge University Press, 2000.

[6] Wertz, J., R. *Spacecraft Attitude Determination and Control*, first Edition, D. Reidel Publishing Company, Dordrecht, Holland, 1978. DOI: https://doi.org/10.1007/978-94-009-9907-7.

[7] Jovanovic, et al. Design and Testing of a Low-cost, Open source, 3-D Printed Air-Bearing-Based Attitude Simulator for CubeSat Satellites, *Journal of Small Satellites*, 8(2):859:880, January 2019.

[8] Fleming, A. et al. Minimum-time Reorientation of a Rigid Body, *Journal of Guidance, Control and Dynamic*s, 23(1), January-February 2010. DOI: 10.2514/1.43549.

[9] Weston, S, editor. Small Spacecraft Technology. State of the Art Report. Small Spacecraft Systems Virtual Institute, NASA, California, 2023.

[10] Krishna, N. et al. Design and Implementation of a Reaction Wheel System for CubeSats, IEEE Xplore, Manipal, India. 2018.

[11] K. Ogata, *"Modern Control Engineering",* Fifth Edition. Pearson Education International, Madrid, 2010.

[12] 16.31 Feedback Control Systems, Topic 11: Full-State Feedback Control. MIT OpenCourseWare, https://ocw.mit.edu/courses/16-30-feedback-control-systems-fall-2010/c553561f63feaa6173e31994f45f0c60_MIT16_30F10_lec11.pdf, 2010.

[13] Are brushed motors suitable for industrial applications. Linear Motion Tips, https://www.linear-motiontips.com/are-brushed-motors-suitable-for-industrial-applications/.

[14] Brushed DC Motors Vs. Brushless DC Motors. Hare Data Electronics,

https://www.haredataelectronics.co.uk/brushed-dc-motors-vs-brushless-dc-motors, July 2020.

[15] Krause, P. et al. *Analysis of Electric Machinery and Drive Systems*, IEEE, pp. 557-601. DOI: 10.1109/9780470544167.ch15.

[16] Hanselman, D. *Brushless Permanent Magnet Motor Design*, Second Edition. Magna Physics Publishing, Ohio, U.S.A, 2006.

[17] iPower Moto GM3506 Brushless Gimbal Motor w/ AS5048A Encoder. RobotShop, https://uk.robotshop.com/products/ipower-motor-gm3506-brushless-gimbal-motor-w-as5048a-encoder.

[18] Curtis, H. Orbital Mechanics for Engineering Students, Butterworth-Heinemann, 2014. DOI: https://doi-org.surrey.idm.oclc.org/10.1016/C2011-0-69685-1.

[19] Orbital Mechanics & Astrodynamics. Bryan weber, https://orbital-mechanics.space/intro.html,June 2024.

[20] Place: Pole Placement Design. MathWorks, Help Center, https://uk.mathworks.com/help/control/ref/place.html#mw_00c2ad51-c4f9-46ce-9af1-9465ecfe2af6.

[21] Green, C. and McDonald, R. *Modeling and Test of the Efficiency of Electronic speed controllers for Brushless DC Motors*, Session: Transformational Flight – Electric Propulsion, AIAA 2015-3191, June 2015. DOI: https://doi.org/10.2514/6.2015-3191.

[22] Sidi, M. *Spacecraft dynamics and control: a practical engineering approach*, Eight Edition, MLA, Cambridge University Press, 1997.

8 APPENDIX

8.1 APPENDIX A: Coordinate System Definition (CSD) Document
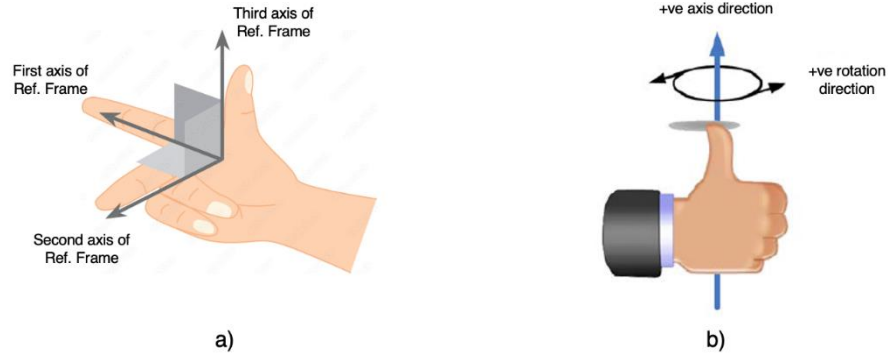
Figure 8-1: Right hand Rule.

1. Overview of Coordinate Systems

1.1 Summary

Table 1: Summary of coordinate systems.

Title	Mnemonic	ID
Flight/Astronomical Frames		
Granite Table Inertial Coordinate System	GTI	F-01
Robot Trajectory System (Robot Orbital Frame)	RTS	F-02
Mechanical		
Body Centred Reference Frame	BFR	M-01
Mechanical Reference Frame (CAD)	CAD	M-02
Reaction Wheel Frame	RWF	M-B-01
Camera Reference Frame	CAM	M-B-02
Inertial Sensor Reference Frame	IMU	M-B-03

1.2 Frank Diagram
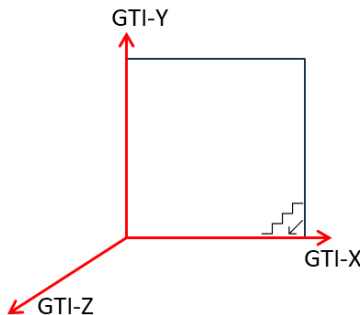
Figure 8-2. Frank Diagram. "T" stands for translation, "R" for rotation and "A" refers to the Attitude Dynamics equations.

2. Coordinate Systems

2.1 Attitude Reference Frames

2.1.1 *Table Fixed Coordinate System*

Table 2: RCF Definition

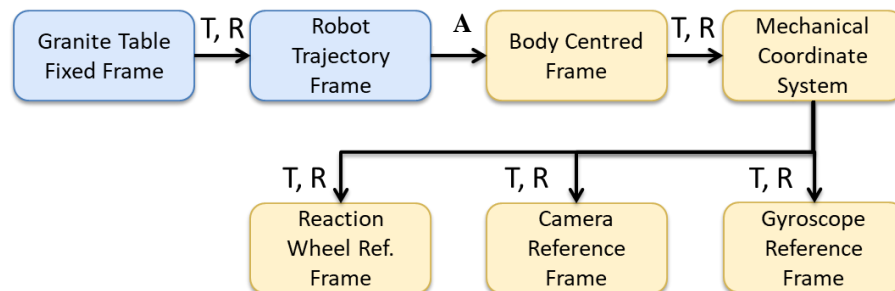| Type	Title	Mnemonic	ID
Fixed	Granite Table Inertial Coordinate System	GTI	F-01
Definition:			
+X_GTI	The X axis is aligned to the nearest short axis of table. Pointing to the right.		
+Y_GTI	The Y axis is aligned to the left long axis of the table.		
+Z_GTI	Completes the triad (90 deg). The positive direction is away from the surface of the Earth. (Points to the roof).		
Origin	Left front corner of the room.		
Rationale: The orbit of the robot is defined and calculated in the GTI frame.			
Transformation: -			
Translation: -			
Rotation: -			
Order: -			
Comments			
Formula: -			
Diagram:			

Figure 8-3: GTS reference frame.

2.1.2 *Robot Trajectory Coordinate System (Robot Orbital Frame)*

Table 3: RTS definition

Type	Title	Mnemonic	ID
Translational Frame	Robot Trajectory Coordinate System	RTS	F-02
Definition:			
+X_RTS	Completes the triad (90 deg).		
+Y_RTS	The Y axis pointing to the velocity direction of the robot.		
+Z_RTS	The Z-axis is aligned to the Z-axis of the Table Frame.		
Origin	Centre of mass of the Robot		

Rationale:

Transformation: - Granite Table Inertial Coordinate System (GCI)

Translation: - Translation along X and Y axis.

Rotation: - Rotation about Z axis through a variable angle. Through an angle equal to the angle between +GTI_Y and the velocity trajectory.

Order: -

Comments: W in Translation matrix is the distance from the base of the Granite Table to the centre of mass of the Robot in the RTS_Z axis.

Formula: -

$$\begin{bmatrix} X \\ Y \\ Z \end{bmatrix}_{RTS} = \begin{bmatrix} \cos\theta & \sin\theta & 0 \\ -\sin\theta & \cos\theta & 0 \\ 0 & 0 & 1 \end{bmatrix} \begin{bmatrix} x \\ y \\ z \end{bmatrix}_{GTI}^{Rotation} + \begin{bmatrix} x' \\ y' \\ W \end{bmatrix}_{GTI}^{Translation}$$

Diagram:

Figure 8-4: RTS Reference Frame.

2.2 Mechanical Frames

2.2.1 *Body-fixed Reference Frame*

Table 4: Body-Fixed Frame definition

Type	Title	Mnemonic	ID
Rotating Reference Frame	Body-fixed Reference Frame	BFR	M-01
Definition:			
+X_BFR	The X axis points UP, where the minimum Moment of Inertia relies.		
+Y_BFR	The Y axis points to the FRONT side of the robot.		
+Z_BFR	The Z axis completes the triad.		
Origin	Centre of mass of the robot.		

Rationale: This frame rotates along with the robot. Attitude Matrix describe the position of the body frame in the room. The actual vertical distance from the table and the Centre of Mass of the robot is W=0.1344 meters, but it could vary if extra components are added and therefore the position of the Centre of Mass change.

The following matrices are the DCM and Translation matrixes from the Mechanical Frame to the Body Frame.

Transformation: From Mechanical Frame to Body Frame.

Translation: Translation along the three axes: $[0.0190809 \quad 0.00224927 \quad 0.10277103]^T$

Rotation: Rotation about 3 axes from Mechanical Frame to Body Frame:

$$[BM] = \begin{bmatrix} -0.00441177 & 0.97219108 & 0.23414747 \\ -0.00288917 & -0.23416116 & 0.97219350 \\ 0.99998609 & -0.00361260 & 0.00384189 \end{bmatrix}$$

Order: -

Comments:

Formula:

$$\begin{bmatrix} X \\ Y \\ Z \end{bmatrix}_{MNT} = \begin{bmatrix} -0.00441177 & 0.97219108 & 0.23414747 \\ -0.00288917 & -0.23416116 & 0.97219350 \\ 0.99998609 & -0.00361260 & 0.00384189 \end{bmatrix} \begin{bmatrix} X \\ Y \\ Z \end{bmatrix}_{CAD} + \begin{bmatrix} 0.0190809 \\ 0.00224927 \\ 0.10277103 \end{bmatrix}$$
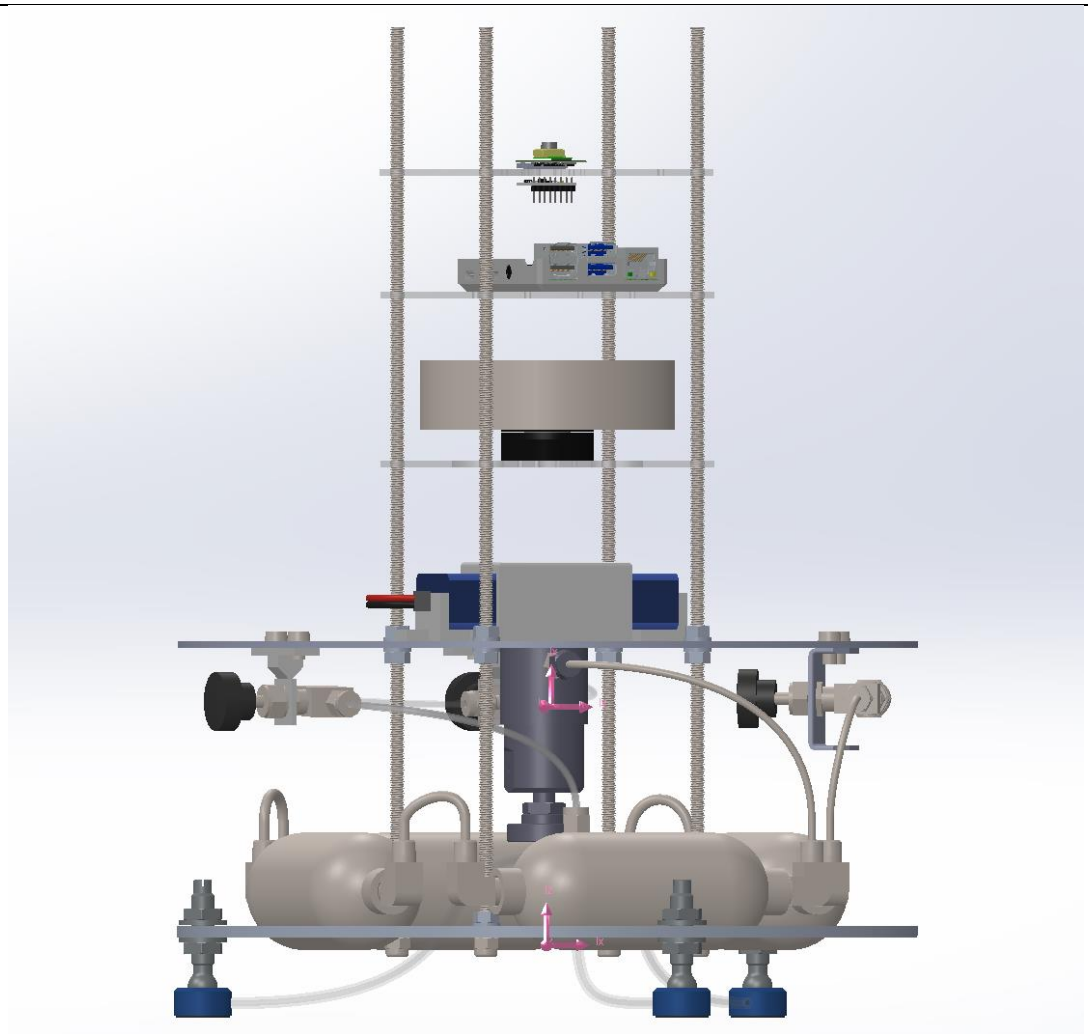
Diagram:

Figure 8-5. Body Fixed Reference Frame & Mechanical CAD Frame Below.

```
Report coordinate values relative to:  Origin Coordinate System              ∨

Mass properties of Floating Robot 2
    Configuration: Predeterminado
    Coordinate system: Origin Coordinate System

Mass = 5.77664482 kilograms

Total weld mass = 0.00000000 kilograms

Volume = 0.00139468 cubic meters

Surface area = 0.85281179 square meters

Center of mass: ( meters )
    X = 0.00190809
    Y = 0.00224927
    Z = 0.10277103

Principal axes of inertia and principal moments of inertia(user-overridden): ( kilograms * square meters )
Taken at the center of mass.
    Ix = ( 0.00454881,  0.00307793,  0.99998492)        Px = 0.05116256
    Iy = ( 0.97224477,  0.23390953, -0.00514260)        Py = 0.08095379
    Iz = (-0.23392183,  0.97225350, -0.00192849)        Pz = 0.08397855

Moments of inertia: ( kilograms * square meters )
Taken at the center of mass and aligned with the output coordinate system. (Using positive tensor notation.)
    Lxx = 0.08111868        Lxy = 0.00068834        Lxz = 0.00013415
    Lyx = 0.00068834        Lyy = 0.08381274        Lyz = 0.00009737
    Lzx = 0.00013415        Lzy = 0.00009737        Lzz = 0.05116347

Moments of inertia: ( kilograms * square meters )
Taken at the output coordinate system. (Using positive tensor notation.)
    Ixx = 0.14216017        Ixy = 0.00071313        Ixz = 0.00126692
    Iyx = 0.00071313        Iyy = 0.14484603        Iyz = 0.00143270
    Izx = 0.00126692        Izy = 0.00143270        Izz = 0.05121373
```
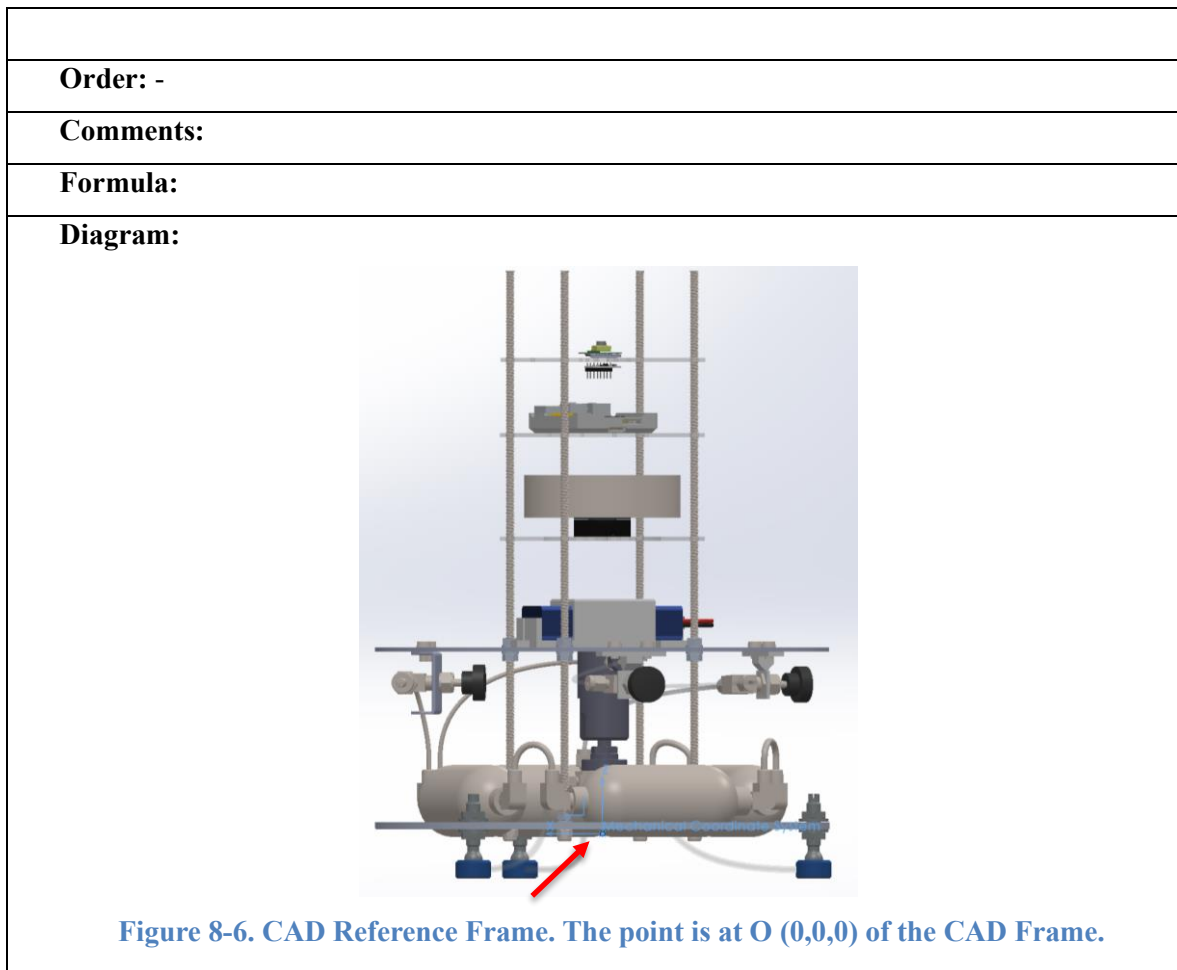
2.2.2 Mechanical CAD Reference Frame

Table 8-5: CAD Reference Frame definition.
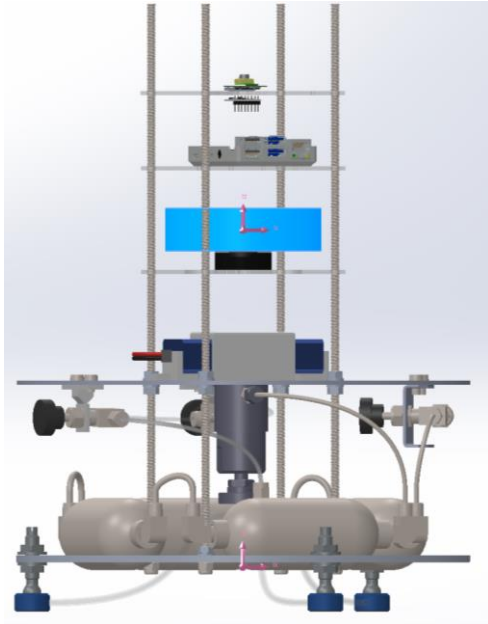
Type	Title	Mnemonic	ID
Rotating Reference Frame	Mechanical Reference Frame	CAD	M-02
Definition:			
+X_CAD	The X axis points to the RIGHT side of the robot.		
+Y_CAD	The Y axis complete the triad.		
+Z_CAD	The Z axis points UP, away from the surface of the table.		
Origin	Origin of CAD File (0,0,0)		
Rationale: This Frame is used to locate the subsequent frames from the Body-Fixed Frame in the 3D CAD model.			
Transformation:			
Translation:			
Rotation:			

Order: -	
Comments:	
Formula:	
Diagram:	

Figure 8-6. CAD Reference Frame. The point is at O (0,0,0) of the CAD Frame.

2.2.3 Reaction Wheel Frame

Table 8-6: IMU Reference definition

Type	Title	Mnemonic	ID
Rotating Reference Frame	Reaction Wheel Frame	RWF	M-B-01
Definition:			
+X_CAM	The X points to one of the sides of the Wheel.		
+Y_CAM	The Y axis completes the Triad.		
+Z_CAM	The Z axis is parallel to the Z axis (+Z_CAD) of the mechanical reference frame		
Origin	Reaction Wheel System Centre of Mass.		
Rationale: The Reaction wheel system is not at the centre of the robot.			
Transformation: From Mechanical CAD to RWF.			
Translation: Translation along the Z axis of the CAD reference frame.			

$[WM_T] = [0 \quad 0 \quad 0.2373]^T \, meters$

Rotation:

Rotation about the Z axis as the Reaction Wheel is a non-inertial frame.

$$[WM]_R = \begin{bmatrix} \cos\psi & \sin\psi & 0 \\ -\sin\psi & \cos\psi & 0 \\ 0 & 0 & 1 \end{bmatrix}$$

Order: $-[WM] = R_3(\psi)$

Comments:

Formula:

$$\begin{bmatrix} X \\ Y \\ Z \end{bmatrix}_{RWF} = \begin{bmatrix} 1 & 0 & 0 \\ 0 & 1 & 0 \\ 0 & 0 & 14 \end{bmatrix} \begin{bmatrix} x \\ y \\ z \end{bmatrix}_{CAD} + \begin{bmatrix} 0 \\ 0 \\ 0.2373 \end{bmatrix}$$

Diagram:

Figure 8-7. Reaction Wheel Frame vs Mechanical CAD Frame.

```
Report coordinate values relative to: Mechanical Coordinate System          ∨

Mass properties of Floating Robot 2
    Configuration: Predeterminado
    Coordinate system: Mechanical Coordinate System

Mass = 5.77664482 kilograms

Total weld mass = 0.00000000 kilograms

Volume = 0.00139468 cubic meters

Surface area = 0.85281179 square meters

Center of mass: ( meters )
    X = 0.00190809
    Y = 0.00224927
    Z = 0.10277103

Principal axes of inertia and principal moments of inertia(user-overridden): ( kilograms * square meters )
Taken at the center of mass.
    Ix = ( 0.00454881,  0.00307793,  0.99998492)        Px = 0.05116256
    Iy = ( 0.97224477,  0.23390953, -0.00514260)        Py = 0.08095379
    Iz = (-0.23392183,  0.97225350, -0.00192849)        Pz = 0.08397855

Moments of inertia: ( kilograms * square meters )
Taken at the center of mass and aligned with the output coordinate system. (Using positive tensor notation.)
    Lxx = 0.08111868        Lxy = 0.00068834        Lxz = 0.00013415
    Lyx = 0.00068834        Lyy = 0.08381274        Lyz = 0.00009737
    Lzx = 0.00013415        Lzy = 0.00009737        Lzz = 0.05116347

Moments of inertia: ( kilograms * square meters )
Taken at the output coordinate system. (Using positive tensor notation.)
    Ixx = 0.14216017        Ixy = 0.00071313        Ixz = 0.00126692
    Iyx = 0.00071313        Iyy = 0.14484603        Iyz = 0.00143270
    Izx = 0.00126692        Izy = 0.00143270        Izz = 0.05121373
```
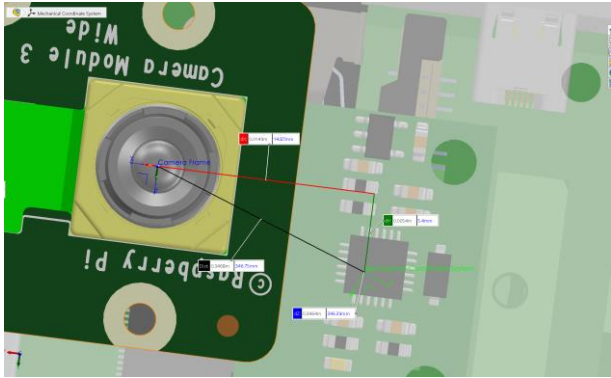
2.2.4   Camera Reference Frame

Table 8-7: CAM Reference Frame

Type	Title	Mnemonic	ID
Fixed Reference Frame	Camera Reference Frame	CAM	M-B-02
Definition:			
+X_CAM	The X axis completes the triad.		
+Y_CAM	The Y axis points downwards the camera.		
+Z_CAM	The Z axis points outside the camera.		
Origin	Image sensor of the camera		
Rationale: The image sensor of the camera is not at the centre of the mount. Real position is obtained from the CAD file.			
Transformation: From Mechanical CAD to CAM.			

Translation: Translation along the three axes of the CAD reference frame.
$$[CM_T] = [0.0180 \quad 0.2436 \quad 0.0011]^T \, meters$$

Rotation: Fixed rotation about the Z axis: $\phi = 67.23 \, deg, \theta = 67.23 \, deg, \psi = 0$
$$[CM] = \begin{bmatrix} 0.3870 & 0.9221 & 0 \\ -0.9221 & 0.3870 & 0 \\ 0 & 0 & 1 \end{bmatrix}$$

Order:

Comments: The size of the translation depends on the model of camera and where the image sensor is positioned with respect to the base of the camera.

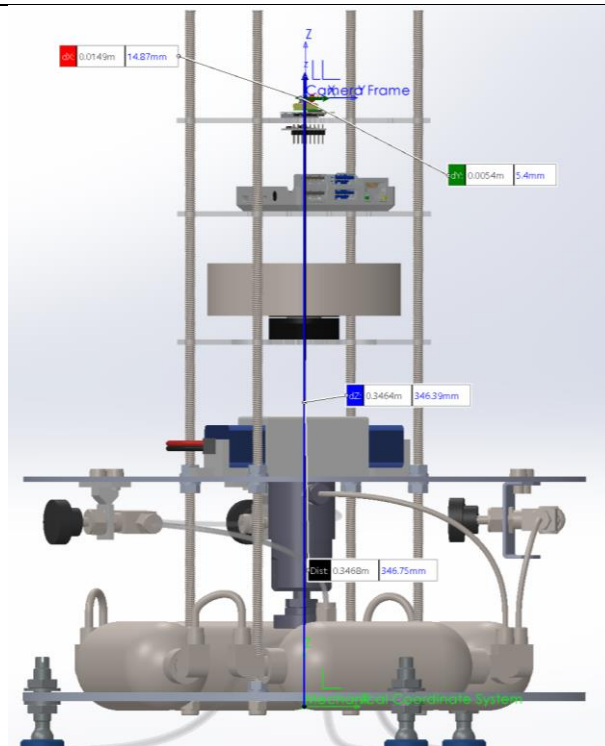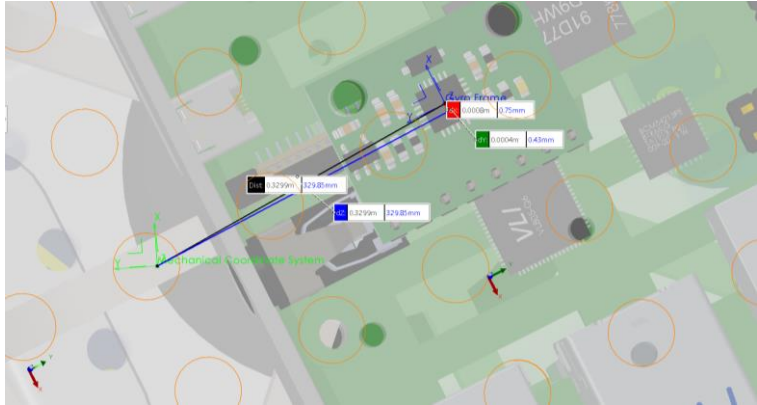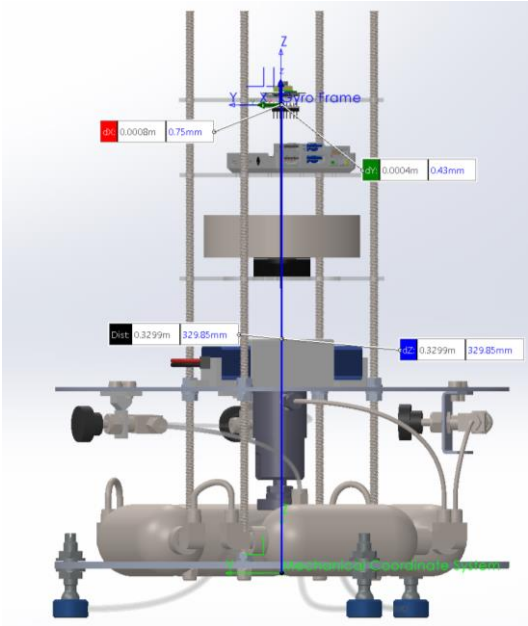| **Formula:** |
|---|
| $$\begin{bmatrix} X \\ Y \\ Z \end{bmatrix}_{CAM} = \begin{bmatrix} 0.3870 & 0.9221 & 0 \\ -0.9221 & 0.3870 & 0 \\ 0 & 0 & 1 \end{bmatrix} \begin{bmatrix} x \\ y \\ z \end{bmatrix}_{CAD}^{Rotation} + \begin{bmatrix} 0.01487 \\ -0.0054 \\ 0.3464 \end{bmatrix}_{CAD}^{Translation}$$ |

Diagram:

Figure 8-8. Camera Reference Frame (CAM), Mechanical Frame (CAD).

2.2.5 *Inertial Sensor Frame*

Table 8-8: IMU Reference definition

Type	Title	Mnemonic	ID
Rotating Reference Frame	Inertial Sensor Reference Frame	IMU	M-B-02
Definition:			
+X_CAM	The X axis is parallel to the X axis (+X_CAD) of the mechanical reference frame		
+Y_CAM	The Y axis is parallel to the Y axis (Y+_CAD) of the mechanical reference frame		
+Z_CAM	The Z axis is parallel to the Z axis (+Z_CAD) of the mechanical reference frame		
Origin	Gyroscope Sensor Centre of Mass.		
Rationale: The gyroscope sensor is not at the centre of the robot.			
Transformation: From Mechanical CAD to IMU (from Mechanical)			
Translation: Translation along the three axes of the CAD reference frame:			

$$[GM]_T = [0.0006 \quad 0.0031 \quad 0.2271]^T \; meters$$

Rotation: Fixed rotation about $\phi = 22.77 \; deg, \theta = 22.77 \; deg, \psi = 0 \; deg.$

$$[GM]_R = \begin{bmatrix} 0.9225 & -0.3859 & 0 \\ -0.3859 & 0.9225 & 0 \\ 0 & 0 & 1 \end{bmatrix}$$

Order: $[GC] = R_3(\phi)$

Comments:

Formula:

$$\begin{bmatrix} X \\ Y \\ Z \end{bmatrix}_{IMU} = \begin{bmatrix} 0.9225 & -0.3859 & 0 \\ -0.3859 & 0.9225 & 0 \\ 0 & 0 & 1 \end{bmatrix} \begin{bmatrix} x \\ y \\ z \end{bmatrix}_{CAD} + \begin{bmatrix} 0.0008 \\ 0.0004 \\ 0.3299 \end{bmatrix} m$$

Diagram:

Figure 8-9. Distance from Mechanical Frame to Gyro Frame

Figure 8-10. Gyroscope Frame and Mechanical CAD Frame.

APPENDIX B: MATLAB Scripts & Simulink Models

All MATLAB Scripts, Simulink Models, Images and code files were submitted to the next GitHub Repository:

https://github.com/JorgeACM/Reaction-Wheel-Control.git.